Journal of Wind Engineering & Industrial Aerodynamics 179 (2018) 319–337

Contents lists available at ScienceDirect

Journal of Wind Engineering & Industrial Aerodynamics

journal homepage: www.elsevier.com/locate/jweia

Aerodynamic drag in cycling pelotons: New insights by CFD simulation and wind tunnel testing

Bert Blocken [a,b,*], Thijs van Druenen [a], Yasin Toparlar [a], Fabio Malizia [b], Paul Mannion [a,c,d], Thomas Andrianne [e], Thierry Marchal [f], Geert-Jan Maas [a], Jan Diepens [a]

[a] Department of the Built Environment, Eindhoven University of Technology, P.O. Box 513, 5600, Eindhoven, the Netherlands
[b] Department of Civil Engineering, KU Leuven, Kasteelpark Arenberg 40 – Bus 2447, 3001, Leuven, Belgium
[c] Department of Civil Engineering, National University of Ireland Galway, University Road, Galway, Ireland
[d] Informatics Research Unit for Sustainable Engineering (IRUSE), Ireland
[e] Department of Aerospace and Mechanical Engineering, University of Liège, Allée de la Découverte, 9 Quartier Polytech 1, B52/3. B-4000 Liège, Belgium
[f] ANSYS Belgium S.A., Centre d'Affaires "Les Collines de Wavre", Avenue Pasteur 4, 1300, Wavre, Belgium

ARTICLE INFO

Keywords:
Cycling aerodynamics
Computational fluid dynamics
Wind tunnel testing
Aerodynamic resistance
Sports

ABSTRACT

A cycling peloton is the main group of cyclists riding closely together to reduce aerodynamic drag and energy expenditure. Previous studies on small groups of in-line drafting cyclists showed reductions down to 70 to 50% the drag of an isolated rider at same speed and these values have also been used for pelotons. However, inside a tightly packed peloton with multiple rows of riders providing shelter, larger drag reductions can be expected. This paper systematically investigates the drag reductions in two pelotons of 121 cyclists. High-resolution CFD simulations are performed with the RANS equations and the Transition SST-k-ω model. The cyclist wall-adjacent cell size is 20 μm and the total cell count per peloton is nearly 3 billion. The simulations are validated by four wind-tunnel tests, including one with a peloton of 121 models. The results show that the drag of all cyclists in the peloton decreases compared to that of an isolated rider. In the mid rear of the peloton it reduces down to 5%–10% that of an isolated rider. This corresponds to an "equivalent cycling speed" that is 4.5 to 3.2 times less than the peloton speed. These results can be used to improve cycling strategies.

1. Introduction

A cycling peloton is the main group of cyclists riding closely together to reduce aerodynamic drag and energy expenditure (Fig. 1). It is well known that the riders in front experience the largest drag. Therefore, after riding some time at the front, these riders will move farther back in the peloton to recover and others will take over. Generally, the leaders and/or sprinters of each team will not ride in front, but stay embedded somewhere inside the peloton to save as much energy as possible until the most critical part of the race. This critical part can be a long climb or another event that can break the peloton into pieces. It can also be the moment near the end of the race where the peloton will rapidly change shape to prepare for the sprint towards the finish line. For long multi-stage races like the Tour de France, the Giro d'Italia or the Vuelta d'España, endurance and a low level of fatigue during the third week of the race is critical to win. Therefore, athletes are continuously focused on preserving energy for the critical days like mountain stages or time trials. Hence, the peloton is used to obtain shelter from the wind and limit energy consumption. While it is well known that the aerodynamic drag inside the peloton is significantly less than that at the front, it is not known how much this drag inside the peloton actually decreases and which positions are most beneficial in terms of drag reduction. It is also not known how much the drag is for the riders at the front of the peloton.

The greatest potential for improvement in cycling speed is situated in the aerodynamics (Wilson, 2004). At racing speeds (about 54 km/h or 15 m/s in a competitive cycling event), the aerodynamic resistance or drag is about 90% of the total resistance (Kyle and Burke, 1984; Grappe et al., 1997; Lukes et al., 2005). Aerodynamic drag can be assessed by field tests, by wind tunnel measurements or by numerical simulation with Computational Fluid Dynamics (CFD). The use of CFD in wind engineering, also referred to as Computational Wind Engineering, has seen a rapid growth in the past 50 years (see review papers of e.g. Murakami, 1997, Stathopoulos, 1997, Baker, 2007, Solari, 2007, Meroney and Derickson, 2014, Blocken, 2014, 2015). As part of wind engineering, also

* Corresponding author. Department of the Built Environment, Eindhoven University of Technology, P.O.Box 513, 5600 MB, Eindhoven, The Netherlands.
E-mail address: b.j.e.blocken@tue.nl (B. Blocken).

https://doi.org/10.1016/j.jweia.2018.06.011
Received 27 May 2018; Received in revised form 1 June 2018; Accepted 21 June 2018

Fig. 1. Cycling pelotons. Sources: (a,b) Sporza.be; (c) http://johnericgoff.blogspot.com; (d) Sporza.be; (e) Sergii Rudiuk / Shutterstock.com, reproduced with permission; (f) www.danpontefract.com; (g) (c) Cor Vos, reproduced with permission; (h) Getty Images, reproduced with permission.

the field of cycling aerodynamics has adopted the use of CFD (Blocken, 2014; Crouch et al., 2017).

Most studies on cycling aerodynamics focused on the drag of a single (isolated) cyclist (e.g. Kyle and Burke, 1984; Dal Monte et al., 1987, Grappe et al., 1997; Padilla et al., 2000; Jeukendrup and Martin, 2001; Defraeye et al., 2010a, 2010b; Crouch et al., 2014; Fintelman et al., 2014, 2015). Less attention has been given to analyzing the effects of drafting. In drafting, two or more cyclists ride close behind each other to reduce aerodynamic drag. This way, the trailing cyclist can benefit from the low pressure area behind the leading cyclist. Early drafting studies, mostly coast-down tests and wind tunnel experiments, were reported by Kyle (1979), McCole et al. (1990), Hagberg and McCole (1990), Kyle (1991), Broker and Kyle (1995), Zdravkovich et al. (1996), Olds (1998), Martin et al. (1998), Broker et al. (1999), Edwards and Byrnes (2007) and Garcia-Lopez et al. (2008). Broker and Kyle (1995) and Garcia-Lopez et al. (2008) studied the drag of 5 cyclists in time-trial (TT) position while Martin et al. (1998) studied 6 cyclists in TT position. More recently, Blocken et al. (2013) investigated the aerodynamic benefit for a leading cyclist due to the presence of a trailing cyclist based on CFD simulations and wind tunnel measurements. It was found that the trailing cyclist can provide a drag reduction of almost 3% to the leading cyclist due to the upstream effect exerted by the trailing rider on the flow. This effect was later confirmed by Defraeye et al. (2014) and Barry et al. (2015) who studied the aerodynamic drag of four in-line cyclists for a team pursuit. As a special case of drafting, Blocken and Toparlar (2015) assessed the aerodynamic benefit for a cyclist by a following car and Blocken et al. (2016) assessed the aerodynamic benefit for a cyclist followed by one, two or three motorcycles. Mannion et al., 2018a; b also analyzed a special case of drafting, i.e. the interaction between the pilot and the stoker in paralympic tandem cycling, where both athletes are in much closer proximity as in drafting in regular cycling.

However, to the best of our knowledge, studies of aerodynamic drag in large groups of drafting cyclists have not yet been performed. The results of previous investigations of the drag in small in-line groups of

drafting cyclists showed reductions down to 50% the drag of an isolated rider. These results have probably led to the common assumption that drag reductions in the cyclist peloton also go down to about 50% (McCole et al., 1990; Burke, 2003). As an example, in the recently developed mathematical model for a cyclist breaking away from a peloton, Gaul et al. (2018) assume that the drag for a cyclist in the peloton is reduced to 70% compared to that of an isolated rider. This is based on the work by Kyle (1979) that showed that a rider cycling directly behind another rider experiences a drag reduction of about a third. In the development of their mathematical agent-based model of peloton dynamics, Ratamero (2015) correctly states that "there is no extensive study of drafting coefficients when a cyclist is not directly behind another one, as there is scarce data about drafting multiple riders; we only know for sure that drafting behind multiple riders is more beneficial than behind only one".

Indeed, for a cyclist in the mid rear of a tightly packed peloton with multiple rows of riders providing shelter from wind (see Fig. 1), a larger drag reduction can be expected than obtained in simple in-line configurations of only a few riders. A drag reduction down to a value of 70% or 50% that of an isolated rider also does not correspond to the experience expressed by professional cyclists and practical cycling experts, who mention that "a cyclist situated in the belly of the peloton hardly has to pedal to move with the peloton and will have extremely low energy expenditure" (e.g. Bakelants, 2018; Wuyts and De Cauwer, 2018). This apparent contradiction indicates that there is only little scientific information on aerodynamic drag in cycling pelotons. It is not known how much the drag inside the peloton actually decreases and which positions are most beneficial in terms of drag reduction. It is also not known how much drag is experienced by the cyclists riding in front or at the outskirts of the peloton.

This paper, therefore, systematically investigates the aerodynamic drag for every rider in two pelotons of 121 cyclists. The pelotons have two different densities and consist of riders in dropped position. High-resolution CFD simulations are performed with the 3D Reynolds-averaged Navier-Stokes (RANS) equations and the Transition SST k-ω model. The simulations are validated by four different wind tunnel tests, including one for a peloton of 121 quarter-scale models. The results are analyzed in terms of mean velocity, mean pressure coefficient, drag reduction and the "equivalent cycling speed", which we will define as the cycling speed of an isolated rider that would yield the same drag as that of the rider in the peloton.

The paper is structured as follows. Section 2 reports the cyclist geometry and the peloton configurations. Section 3 presents three subconfiguration validation studies. Section 4 outlines the wind tunnel measurements for the peloton configuration. In section 5, the CFD simulations for the isolated cyclist, as a reference for the peloton study, are outlined. Section 6 describes the CFD simulations and the results for the two peloton configurations. Finally, sections 7 (discussion) and 8 (summary and conclusions) conclude the paper.

2. Cyclist geometry and peloton configurations

2.1. Cyclist geometry

The cyclist geometry is obtained by scanning a cyclist in dropped position using an Eva structured 3D light scanner (Artec Europe, 2017). Written consent of the scanned athlete was obtained. The athlete has a height of 1.83 m and a weight of 72 kg. Seven angles specifying the cyclist position on the bicycle are determined as in Fig. 2. The legs of the cyclist are static and both wheels of the bicycle are fixed. The bicycle geometry is simplified, specifically concerning the front forks, wheel hubs and spokes, pedals, cranks and handlebars. Some elements of the bicycle are neglected as they are considered small enough not to influence the characteristic flow around it. These include the chains, sprockets, and also brake and gear cables and mechanisms. The frontal area of the cyclist (including bicycle) is 0.423 m^2.

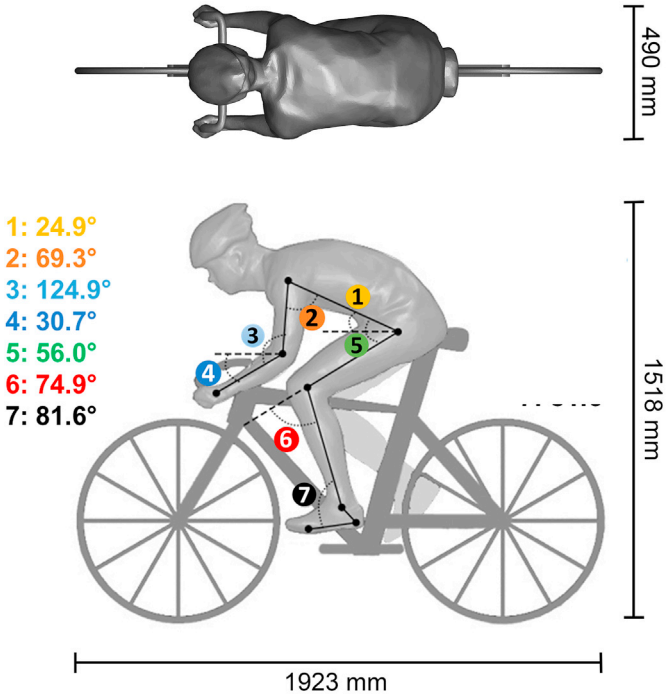

Fig. 2. Cyclist model geometry in dropped position with definition and values of (1) sagittal torso angle; (2) shoulder angle; (3) elbow angle; (4) forearm angle; (5) hip angle; (6) knee angle; (7) ankle angle.

2.2. Peloton configurations

Two peloton configurations are considered, each containing 121 cyclists with geometry as described in section 2.1 (Fig. 3). In each peloton, the cyclists are staggered as common in pelotons (see Fig. 1). Both pelotons consist of 17 rows of cyclists, where the first row contains one cyclist, the second row two cyclists, and so on, up to row 10 with 10 cyclists after which the subsequent rows contain 9 and 10 cyclists alternately, reflecting the maximum number of cyclists in a row as constrained by the width of the road. The two pelotons have different densities. In Peloton A, in side view, the wheels of the cyclists of subsequent rows partially overlap (Fig. 3). In Peloton B, in side view, the wheels do not overlap but are tangential to each other. Peloton A represents a dense peloton while Peloton B represents a sparse one. These two configurations are typical shapes of pelotons progressing at a moderate speed (e.g. 54 km/h) without cross wind or strong head or tail wind and as observed throughout the largest part of the race. A typical example of a dense peloton is given in Fig. 1c and f. The density of atcual pelotons will often be situated somewhere between that of Pelotons A and B (see Fig. 1). Note however that at high speed (e.g. 70 km/h) such as when preparing the sprint in the final part of the race, different peloton configurations will occur that are not studied here as they are only representative of a very small part of the race.

3. CFD subconfiguration validation

3.1. Model configurations

Three model configurations that can be considered as subconfigurations of the peloton configurations are considered for so-called subconfiguration validation as also applied in building and urban aerodynamics (e.g. Franke et al., 2007; Tominaga et al., 2008; Blocken and Carmeliet, 2008; Blocken et al., 2012; Blocken, 2015). The philosophy of subconfiguration validation is to perform the validation on geometrical configurations that are a part of the actual configuration under study. If a given set of computational parameters (domain, grid, approximate form

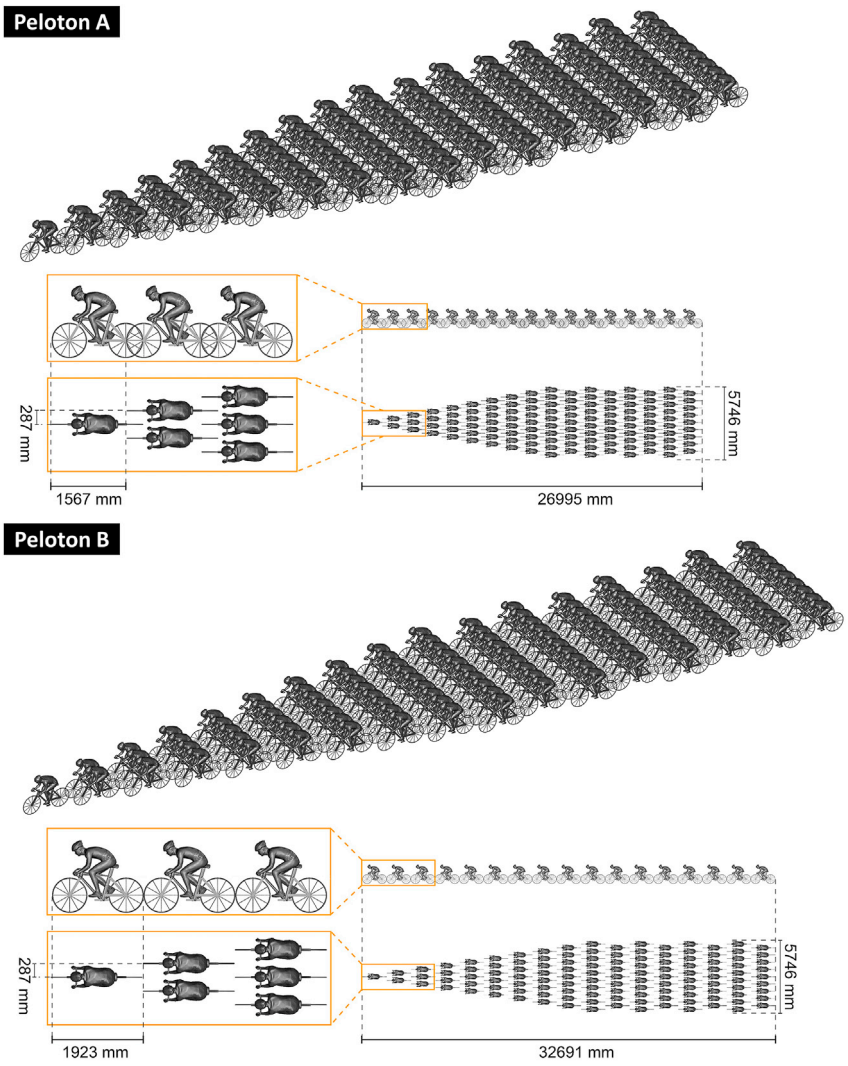

Fig. 3. The two peloton configurations, Peloton A and Peloton B, with 121 cyclists each. Every cyclist has the geometry shown in Fig. 2.

of governing equations, solver settings, etc) yields accurate and reliable results for the subconfigurations, it can reasonable be assumed that the same set of computational parameters will also yield accurate and reliable results for the actual configuration. The cyclist geometry in these subconfigurations is a simplified geometry that is slightly different from that presented in section 2, see Fig. 4. Fig. 5 shows the three subconfigurations. Subconfiguration 1 is a group of 4 drafting cyclists in diamond arrangement that corresponds to the first two rows of cyclists of Peloton B together with the middle cyclist of row three. Subconfiguration 2 is a group of 3 cyclists drafting in-line with wheel-to-wheel separation distance $d = 0.50$ m. Subconfiguration 3 is a group of 4 cyclists drafting in-line with separation distance $d = 0.15$ m. The cyclists are riding at 15 m/s without cross wind, head or tail wind.

3.2. Wind tunnel measurements

The wind tunnel measurements for the three subconfigurations were performed in the aeronautical section of the Wind Tunnel Laboratory at the University of Liège in Belgium. The cross-section of the test section is W x H = $2 \times 1.5\ m^2$. A dedicated set-up with an elevated sharp-edge horizontal plate was developed to limit boundary layer development (Fig. 6). A commercially available force balance was embedded in this set-up. To fully accommodate the models in the wind tunnel at a blockage ratio below 5%, they were manufactured at quarter-scale. The geometry of Fig. 4 was equipped with a bottom plate and with two reinforcement bars connecting the wheels to the bottom plate to ensure sufficient strength and stiffness for testing at 60 m/s. Fig. 7 shows some of the models in the wind tunnel. Tests were performed at 60 m/s to ensure Reynolds number similarity with the (full-scale) CFD simulations and with reality at 15 m/s cycling speed. The drag force, i.e. the horizontal force component parallel to the wind direction and bicycle, was measured using a force transducer with a conservative maximum error estimate of 1.24 N with 95% confidence level, although the actual precision is expected to be much better (Gore, 2016). It should be noted that this error includes both systematic and random errors, and that systematic errors were removed by biasing prior to every measurement. The data were sampled at 10 Hz for 180 s after an initial settling period of 30 s. During the measurements, air temperature, wind speed and atmospheric pressure were recorded and the measurement values were adjusted to correspond to the references values of 15 °C, 15 m/s and 101325 Pa as in the CFD simulations. The measurements were also corrected by subtracting the drag of the base plate (see Fig. 7) as well as for blockage using the expressions for solid blockage by Barlow et al. (1999). The boundary-layer height was 6 cm, which is below the feet and pedals of the cyclist. The level of turbulence of the approach flow was lower than 0.2%. The measurement results will be reported together with the simulation results in the next sections.

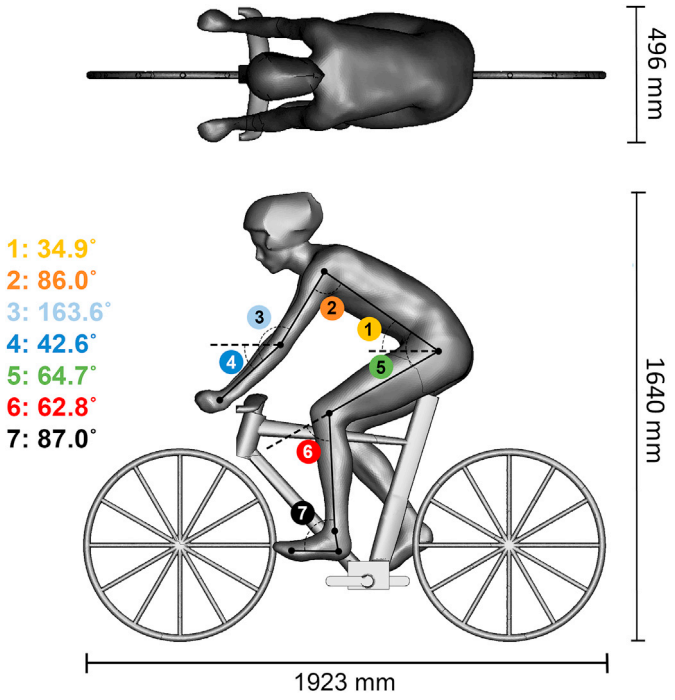

Fig. 4. Simplified cyclist geometry for subconfiguration validation studies with definition and values of (1) sagittal torso angle; (2) shoulder angle; (3) elbow angle; (4) forearm angle; (5) hip angle; (6) knee angle; (7) ankle angle.

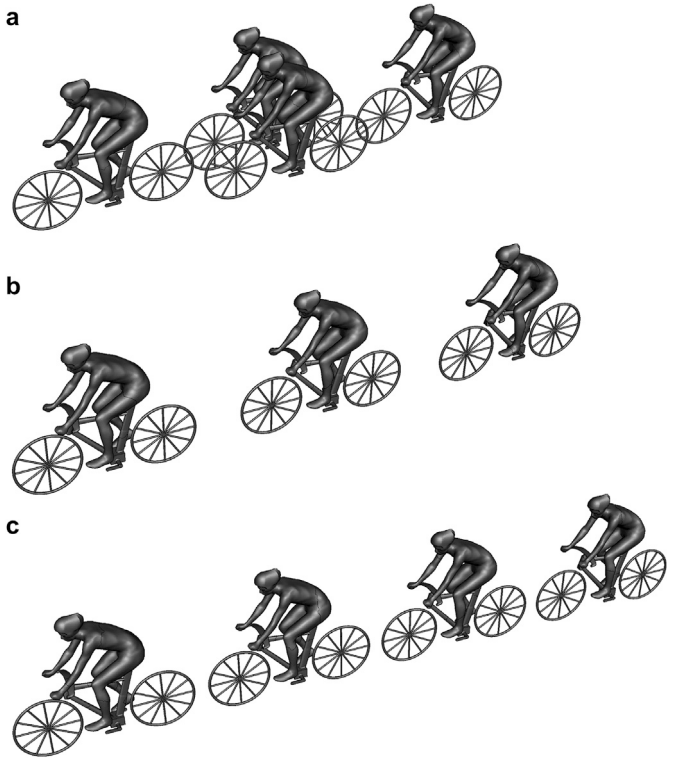

Fig. 5. Three subconfigurations for validation. (a) Diamond configuration similar to the configuration of the first four cyclists in Peloton B; (b) In-line configuration of three cyclists with wheel-to-wheel distance of 0.50 m in full scale; (c) In-line configuration of four cyclists with wheel-to-wheel distance of 0.15 m in full scale.

3.3. Computational domains

The CFD simulations are conducted at full scale. Four simulations are performed, one for the isolated cyclist and three for the subconfigurations. The cyclist models are placed in computational domains with size exceeding the minimum requirements of the best practice guidelines (Franke et al., 2007; Tominaga et al., 2008). The sizes of the domains are L x B x H = $33.8 \times 16.5 \times 9.7\,m^3$ for the isolated cyclist, L x W x H = $37.6 \times 16.5 \times 9.7\,m^3$ for subconfiguration 1, L x W x H = $45.5 \times 17.5 \times 18\,m^3$ for subconfiguration 2, and L x W x H = $46.7 \times 17.5 \times 18\,m^3$ for subconfiguration 3. The maximum blockage ratio is 0.8%, which is well below the recommended maximum value of 3% (Franke et al., 2007; Tominaga et al., 2008). Given this low blockage ratio, the CFD simulations are not corrected for blockage. Note that the distance of the inlet plane to the leading cyclist was chosen sufficiently large (i.e. at least 7.8 m), which is larger than in the best practice guidelines, in order to avoid pressure gradients in/near the inlet plane.

3.4. Computational grids

The grids are based on an extensive grid sensitivity analysis (not reported here) and on grid generation guidelines in CFD (Casey and Wintergerste, 2000; Tucker and Mosquera, 2001; Franke et al., 2007; Tominaga et al., 2008) (Fig. 8). The grid sensitivity analysis indicates the requirement for a wall-adjacent cell size of 20 μm at the cyclist and bicycle surfaces and a prismatic boundary layer mesh of 40 layers of incremental thickness with a maximum growth ratio of 1.1 (Fig. 8a). The small wall-adjacent cell size and the 40 layers are important to fully resolve the thin viscous/laminar sublayer of the boundary layer and the buffer layer, which is important to correctly reproduce boundary layer separation and laminar-to-turbulent transition. The dimensionless wall unit y* is generally lower than 1, although very locally a maximum value of 5 is obtained. Outside the 40 layers, tetrahedral and/or prismatic cells are used. The grids for the isolated cyclist and for the subconfigurations 1, 2 and 3 contain 30, 569, 029 cells, 91, 122, 297 cells, 71, 979, 423 cells and 93, 852, 964 cells, respectively (Fig. 8b–d).

3.5. Boundary conditions

At the inlet, a uniform velocity of 15 m/s and a turbulence intensity of 0.5% are imposed. The latter corresponds to the measured streamwise turbulence intensity of 0.2% together with the assumption that 60% of the total turbulence intensity is contributed by its vertical and lateral components. The cyclist body surfaces are modeled as no-slip walls with a geometric roughness height of 0.1 mm in full scale (corresponding to the estimated 0.025 mm geometric roughness of the models). The bicycle surfaces are modeled as smooth no-slip walls (zero roughness). For the bottom boundary of the domain, a slip wall is defined. For the side and top boundaries of the domain, symmetry conditions are imposed. At the outlet, zero static gauge pressure is imposed.

3.6. Approximate form of the governing equations, turbulence model and solver settings

The 3D RANS equations are solved with the Langtry-Menter 4-equation Transition Shear Stress Transport (SST) k-ω model (Menter et al., 2006; Langtry and Menter, 2009). This turbulence model, also known as the γ-Re_θ model, is implemented in ANSYS 15 and 16 (ANSYS, 2015) and is based on the coupling of the SST k-ω transport equations with two additional transport equations, one for the intermittency and one for the transition onset criteria, in terms of momentum thickness and Reynolds number. The Transition SST model can be used in combination with rough walls by a roughness correlation requiring the geometrical roughness height. The model is applied here with this roughness correlation, with inclusion of curvature correction and with production limiters (ANSYS, 2015). Pressure-velocity coupling is taken care of with the

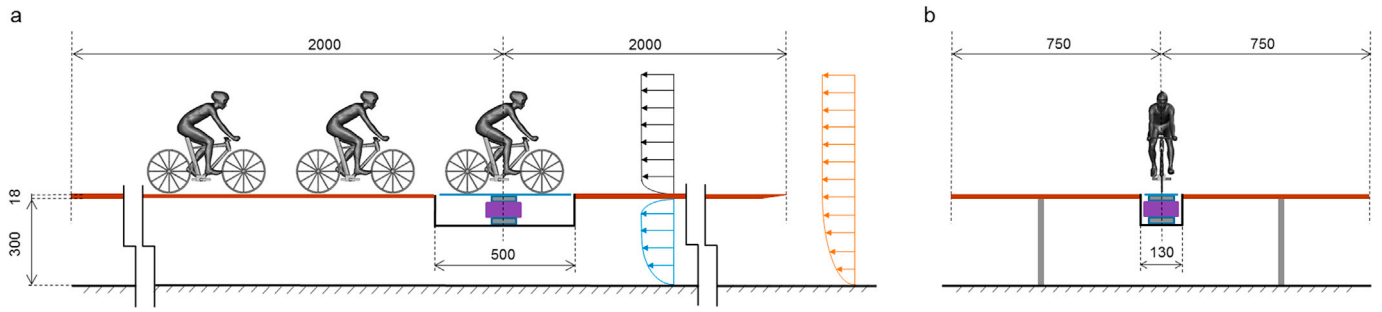

Fig. 6. Wind tunnel set-up at the University of Liège for subconfigurations with models on elevated sharp-edged plate to reduce boundary-layer thickness. Dimensions in mm.

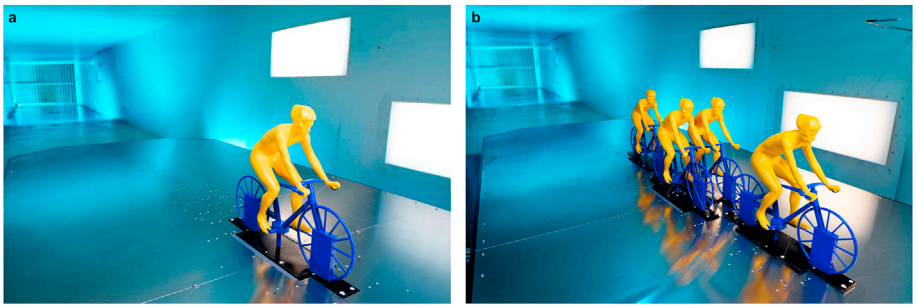

Fig. 7. Photographs of quarter-scale models in wind tunnel: (a) Single cyclist; (b) Diamond configuration.

coupled scheme, pressure interpolation is second order and second-order discretization schemes are used for both the convection terms and the viscous terms of the governing equations. Second order is also applied for the four turbulence model equations. The gradients are computed with the Green-Gauss cell-based method (ANSYS, 2015). The simulations are performed with the commercial CFD code ANSYS Fluent, release 16. The pseudo-transient under-relaxation method is employed with 6000 time steps of 0.01 s. Results are obtained by averaging over the last 5000 pseudo-transient time steps.

3.7. CFD results

Fig. 9 presents the CFD results for the three subconfigurations in terms of contours of mean velocity and mean pressure coefficient. It also shows the value of the drag forces and the drag force percentages relative to the drag force of the isolated rider. The mean pressure coefficient is defined as:

$$C_P = 2\frac{P - P_0}{\rho U_\infty^2} \quad (1)$$

where P is the mean static pressure and P_0 the mean reference static pressure (= atmospheric pressure). The legend in Fig. 9(b,d,f) is limited to the interval [-0.1; 0.1], to more clearly highlight the changes in the static pressure field due to drafting. The drag forces relate to a temperature of 15 °C, a cycling speed of 15 m/s and standard atmospheric pressure of 101325 Pa. The calculated drag force for the isolated rider at the same speed (15 m/s) is 40.33 N. For all subconfigurations, the leading rider has the highest drag, which is either 96% or 98% that of the isolated rider. In subconfiguration 1, the two riders at the second row have a drag that is about 70–75% that of the isolated rider. They each have a different drag, due to the asymmetry of the cyclists (one leg is in front of the other). The trailing rider is shielded by the three leading riders and experiences the lowest drag, which is 43% that of the isolated rider. For subconfiguration 2, the second and third rider have a drag that is 60% and 52% that of the isolated rider, respectively. Finally, for subconfiguration 3, the trailing riders have a monotonically decreasing drag, down to 46% of that of the isolated rider for the fourth in the line. Comparing the drag values of the last rider in every subconfiguration, it is clear that the lowest absolute drag is obtained in the diamond configuration. This already suggests that a rider near the end of a peloton of staggered riders will experience a drag that is substantially lower than that of a rider at the end of a small group of in-line drafting cyclists. Comparing the drag forces for the leading rider in every subconfiguration, the lowest drag is also obtained in the diamond configuration. Blocken et al. (2013) demonstrated earlier that a leading rider enjoys an aerodynamic benefit from riders drafting in his/her wake. This was later also confirmed by studies by Defraeye et al. (2014) and Barry et al. (2015). Blocken et al. (2013) related this effect to the so-called "subsonic upstream disturbance", i.e. the upsteam effect that every obstacle moving in still air has upstream of it. This effect is a direct result of the elliptical mathematical character of the governing partial differential equations for subsonic flow. The leading rider in the diamond configuration has a lower drag than the other leading riders because of the closer proximity of the three trailing riders to this leading rider. The same explanation holds in comparing the drag of the leading rider in Fig. 9c and e, where the one in Fig. 9e has a slightly lower drag.

3.8. Validation

The drag for the isolated cyclist by the wind tunnel measurements is 40.36 N while by CFD it is 40.33 N. This is only a 0.8% difference. However, for the subconfigurations, the differences are larger, as shown in Fig. 10. For subconfiguration 1, the percentage deviations between wind tunnel and CFD are 2.9%, 2.0%, 1.7% and 13.6% for riders C1, C2, C3 and C4, respectively. For subconfiguration 2, the percentage deviations are 2.3%, 1.2% and 5.9% for riders C1, C2 and C3, respectively. For subconfiguration 3, the percentage deviations are 2.9%, 6.0%, 1.3% and 10.8% for riders C1, C2, C3 and C4, respectively. The deviations are largest for the last rider in every subconfiguration, which is likely to be attributed to three reasons: (1) the flow disturbance by the vertical reinforcement plates in the wheels for the wind tunnel tests (see Fig. 7), which are not present in the CFD simulations (see Figs. 4, 5 and 8). This

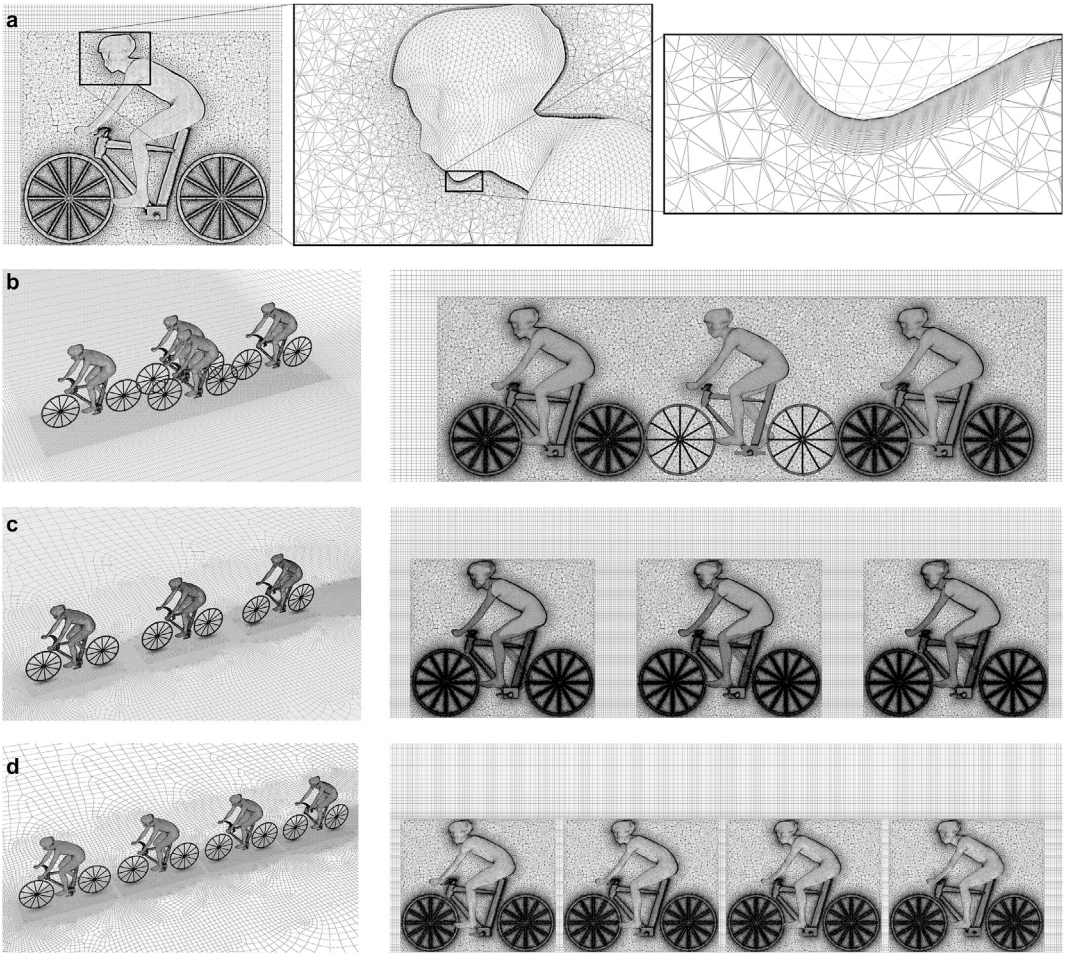

Fig. 8. Computational grids for validation studies: (a) Details of grid topology on cyclist surface and in vertical centerplane; wall-adjacent cell size is 0.02 mm; (b–d) Perspective view and centerplane view for (b) Diamond configuration; 91, 122, 297 cells; (c) In-line configuration of 3 cyclists; 71, 979, 423 cells; (d) In-line configuration of 4 cyclists; 93, 852, 964 cells.

disturbance will accumulate as the flow travels further downstream and is therefore expected to be largest for the last rider in each subconfiguration; (2) the slight vibrations of the cyclist models at the high wind tunnel test speed of 60 m/s; (3) the growing width and increasing transient character of the shear layer with large wind speed gradients when moving further downstream.

4. Wind tunnel measurements for peloton configuration

The wind tunnel measurements for the Peloton A configuration were performed in the Wind Tunnel Laboratory at Eindhoven University of Technology in the Netherlands. The cross-section of the test section is W x H = $3 \times 2\,m^2$. A dedicated set-up with an elevated sharp-edge horizontal plate and embedded force balance was developed to limit boundary layer development (Fig. 11). To fully accommodate the 121 models in the wind tunnel, they were manufactured at quarter-scale, yielding a blockage ratio of 5.7%. Fig. 12 shows the models in the wind tunnel. For the nine models that are situated in the vertical along-wind centerplane, the drag force was measured with a force transducer designed specifically for this experiment and capable of measuring very low drag forces with an accuracy of 0.001 N. This single force transducer was placed alternately below different models. Drag force data were sampled at 127 Hz for 60 s. The tests were performed at 26.7 m/s, which is the maximum wind speed of the facility with the 121 models inside. To enhance Reynolds number independence, the models were manufactured with a specific and rather high geometric surface roughness of 0.25 mm. Reynolds number dependence was tested for every cyclist. The minimum speed for which Reynolds number independence was obtained for every of the nine models in the vertical centerplane was 15 m/s. The level of turbulence of the approach-flow was about 0.3%. The measurements were corrected for blockage using the expressions by Barlow et al. (1999). During the measurements, air temperature, wind speed and atmospheric pressure were recorded and the drag force results were adjusted to match 15 °C, 15 m/s and 101325 Pa which are the values used in the CFD simulations. Fig. 13 shows the measurement results for the nine cyclists in terms of percentage drag of that of an isolated rider at the same speed, i.e. the quarter-scale wind tunnel model tested at 26.7 m/s. It is shown that all nine cyclists benefit from riding in the peloton, even the leading rider (R1), who experiences a drag reduction down to 84% that of the isolated rider. This is caused by the subsonic upstream disturbance by the 120 cyclists drafting in his/her wake. When moving downstream in the peloton, the drag rapidly decreases. Rider R3 only has 35% of the drag of the isolated rider. This value corresponds quite well to that of the trailing rider in Fig. 9b considering that (i) rider R3 has an additional benefit by the 116 riders drafting behind him/her and (ii) the diamond configuration has a larger spacing between the rows than Peloton A. The last four riders, R11 to R17, have a drag force that is below 10% that of the isolated rider. Note that the drag of R15 is lower than that of R17, because R15 still has a few riders behind that yield an additional upstream benefit, which is not the case for R17 who is situated in the last row.

5. CFD simulations for the isolated cyclist

CFD simulations for the isolated cyclist with geometry shown in Fig. 2

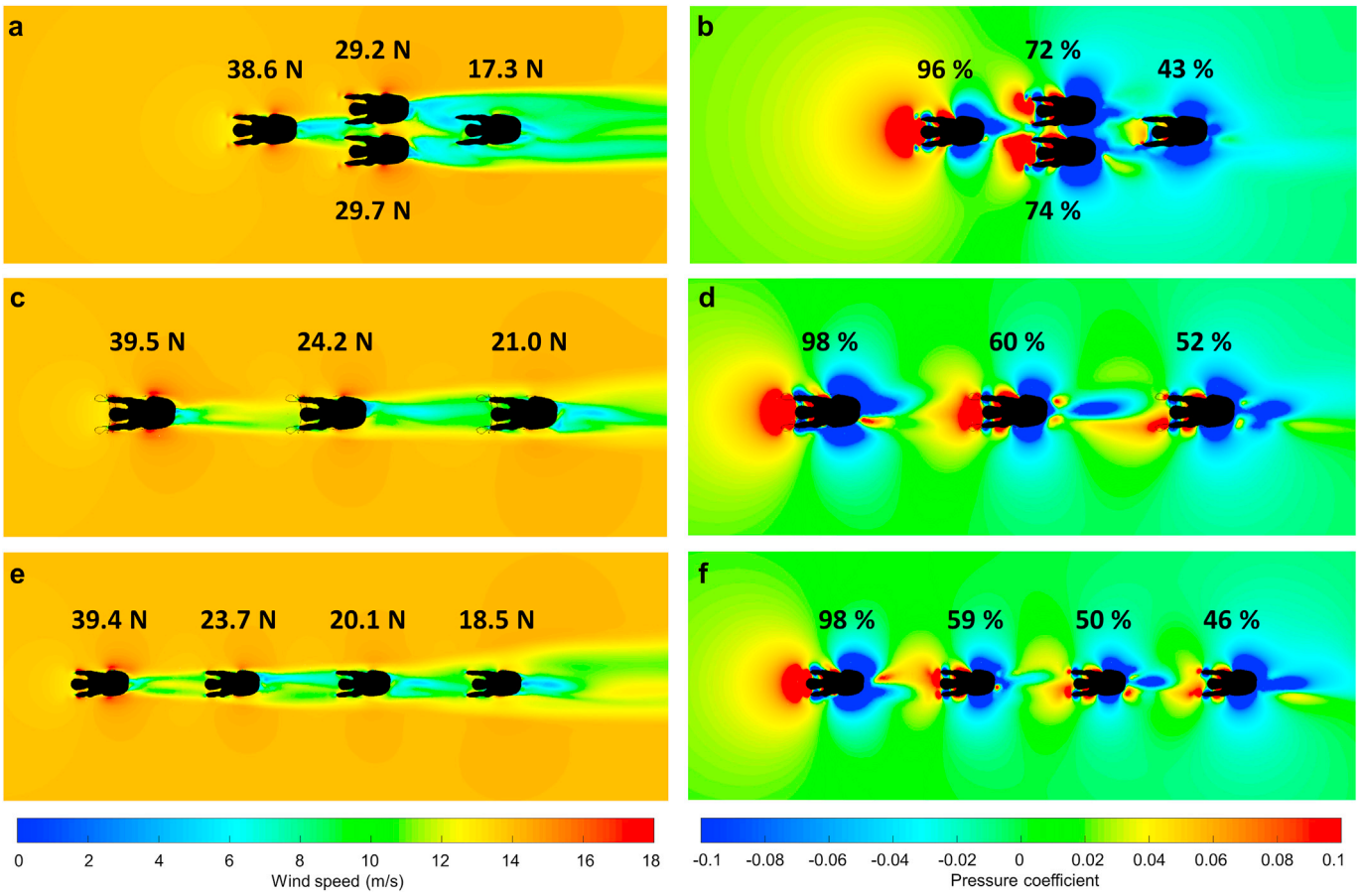

Fig. 9. Contours of (a,c,e) mean wind speed and (b,d,f) mean pressure coefficient in a horizontal plane at 1 m above the road, for the three subconfigurations. Figures a,c,e, also show the values of the drag forces. Figures b,d,f also show the drag as percentage of the drag of an isolated rider at 15 m/s, which is 40.33 N.

are performed as a reference for the CFD evaluation of the drag reductions for the cyclists in the peloton. The computational domain size is L x W x H = $46.7 \times 17.5 \times 18\ m^3$. The computational grid topology is similar as described in section 3.4 and shown in Fig. 14. The boundary conditions, approximate form of the governing equations, turbulence model and solver settings including number of time steps are identical to those mentioned in section 3.6. The resulting drag force for the isolated rider is 37.49 N.

6. CFD simulations for the pelotons

6.1. Computational set-up

The simulations are performed at full scale. Fig. 15 illustrates the computational domains for Pelotons A and B including main dimensions. The computational grids are built with the same topological specifications mentioned before: 20 μm wall-adjacent cells and 40 layers of prisms at the surfaces of every cyclist and every bicycle with stretching ratio below 1.1 (Fig. 14). Due to these stringent grid requirements, the resulting grids contain nearly 3 billion cells for each peloton: 2,979, 420, 781 Peloton A and 2,990, 438, 554 for Peloton B. Fig. 16 shows part of the grid for Peloton A. The boundary conditions are identical to those mentioned in section 3.6. The inlet wind speed (or peloton cycling speed) is 15 m/s, the inlet turbulence intensity is 0.5% and the roughness of the cyclist bodies is 0.1 mm. The bicycle surfaces are considered smooth (zero roughness). The approximate form of the governing equations, turbulence model and solver settings are also identical to those in section 3.6. Given the large number of cells, a larger number of pseudo-transient time steps is needed compared to the subconfiguration validation studies. First, 5000 time steps are employed to reach a statistically steady state. Next, 10,000 time steps are employed over which the resulting data are averaged. The required supercomputing cycles are performed on a Cray XC-40 supercomputer, where for each simulation job one of these four processor group types is used: (1) 484 nodes of Intel(R) Xeon(R) CPU E5-2695 v4 @ 2.10 GHz (Broadwell 18 core at 2.10 GHz); (2) 128 nodes of Intel(R) Xeon(R) CPU E5-2697 v4 @ 2.30 GHz (Broadwell 18 core at 2.30 GHz); (3) 107 nodes of Intel(R) Xeon(R) CPU E5-2698 v4 @ 2.20 GHz (Broadwell 20 core at 2.20 GHz); (4) 160 nodes of Intel(R) Xeon(R) CPU E5-2699 v4 @ 2.20 GHz (Broadwell 22 core at 2.20 GHz). Each node has 128 GB of memory. Each job is run with 13,824 MPI ranks mapped one rank to one core. Each job only places 36 ranks per node. The number of nodes utilized per job is 13,824/36 = 384 nodes. Total memory used is 49,152 GB. Each peloton case took about 54 h to run, a large part of which was used for writing output files.

6.2. Results: mean velocity and mean pressure coefficients

Fig. 17 displays contours of mean wind speed and mean pressure coefficient in a horizontal plane at 1 m above the road surface and in the vertical centerplane for both pelotons. The legend for the pressure coefficient is limited to the interval [-0.1; 0.1] to more clearly highlight the changes in the mean static pressure field. The same is done for all subsequent figures showing mean pressure coefficients. The figures demonstrate that the computational domains are large enough to avoid a significant influence of the inlet, outlet, side walls and top of the domain on the resulting flow parameters in and around the peloton. The contours of mean pressure coefficient show a static pressure above reference static pressure for the front part of the peloton, but a static pressure below reference pressure for the rear part.

Fig. 18 is a detailed view of the same parameters in the same

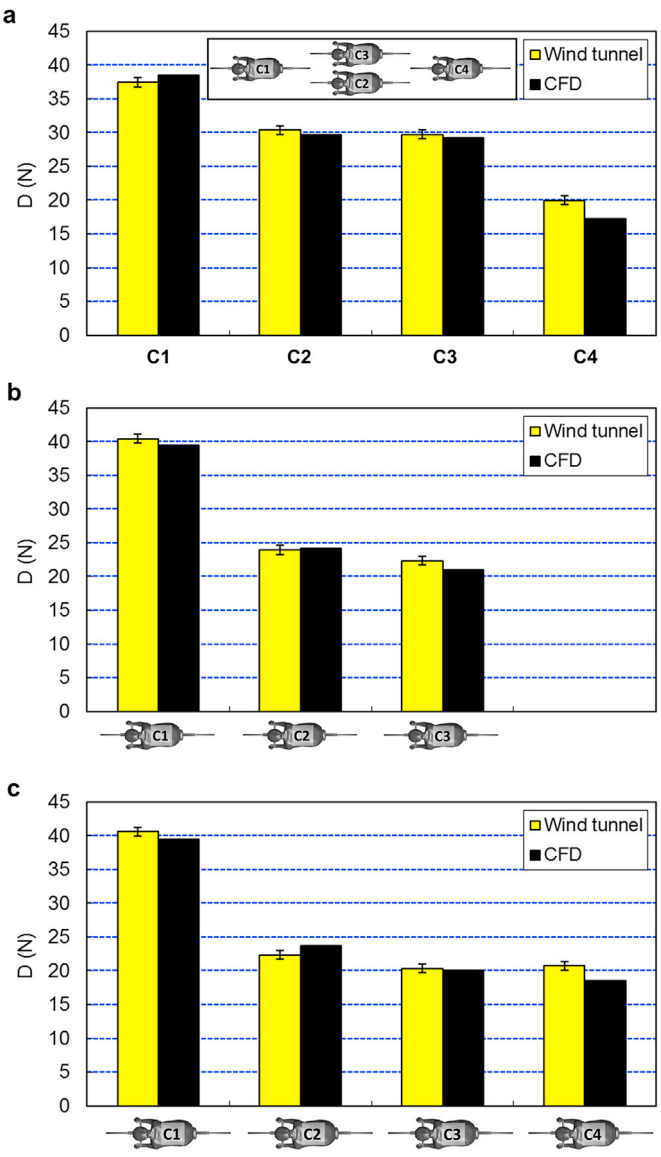

Fig. 10. Results of subconfiguration validation: comparison of drag forces by wind tunnel and CFD for the three subconfigurations.

horizontal and vertical planes. In the peloton, a complex wake flow develops as the combination of the individual wakes behind every cyclist. The resulting air velocities in this wake decrease to less than 3 m/s, which is less than 20% of the actual peloton speed of 15 m/s. The largest static pressure increase occurs in front of the leading cyclist and for the cyclists at the front outer edges of the peloton. The largest static pressure decrease occurs at the rear outer edges of the peloton and behind the last two rows of cyclists.

6.3. Results: validation

Fig. 19 compares the wind tunnel and CFD results of the drag reduction of the nine cyclist in the vertical centerplane. A close agreement is obtained for the first four to five riders, while larger relative differences are obtained for the last four riders. This can be attributed to possible very minor misalignments of the cyclist models but more likely to the complexity of reproducing the shear layers emanating from the riders in the rear part of the peloton. The lowest percentage drag obtained by wind tunnel testing is 7%, while by CFD this is 5%. However, this minimum is found at different positions, for the wind tunnel test at R15 and for the CFD simulations at R17. Nevertheless, both wind tunnel and CFD indicate that the drag of the last four riders is between 5 and 10% that of the isolated rider.

6.4. Results: drag force distribution

Figs. 20 and 21 show the drag force of every rider in Peloton A and B, respectively, as a percentage of the drag force of the isolated cyclist riding at the same speed. Note that these results have a pronounced asymmetry due to the fact that all riders have the same asymmetric leg position (Fig. 2). This situation where all cyclists have static legs with the same asymmetry is not very realistic. Earlier research has shown that the aerodynamic drag of a pedaling cyclist, averaged over one pedaling revolution, is quite similar to that of the same cyclist with the crank almost horizontal (Crouch et al., 2016). Therefore, to increase the realistic character of the study, in Figs. 22 and 23, the results of Figs. 20 and 21 are mirrored around the vertical centerplane and then the original and the mirrored results are averaged to represent the drag experienced over one pedaling revolution. These results are explained below.

Fig. 22 displays the results for Peloton A. Unsurprisingly, the largest drag in the peloton is experienced by the leading rider, who however experiences a reduction in drag down to a value of 86% that of the isolated cyclist riding at the same speed. The cyclists at the outer front edges of the peloton – leading rider excluded – have a drag reduction down to a value in the range of 59–67% that of the isolated rider. For riders sufficiently embedded inside the peloton, the aerodynamic drag rapidly decreases. The riders near the center of the four last rows have the lowest drag. Their resulting drag can go down to only 5% of that of the isolated rider. Overall, the cyclists at the mid rear of the peloton have the strongest drag reductions. 57 of these riders have drag reductions down to 5–10% that of the isolated rider. This means that almost half of this peloton travels at very low cost in terms of energy.

Fig. 23 shows similar results for Peloton B. Because of the larger spacing between the rows in Peloton B, the drag reduction of the leading rider is less, it goes down to only 94% of the value of the isolated cyclist. The cyclists at the outer front edges – leading rider excluded – have a drag reduction to a value in the range of 61%–67%, very similar to Peloton A.

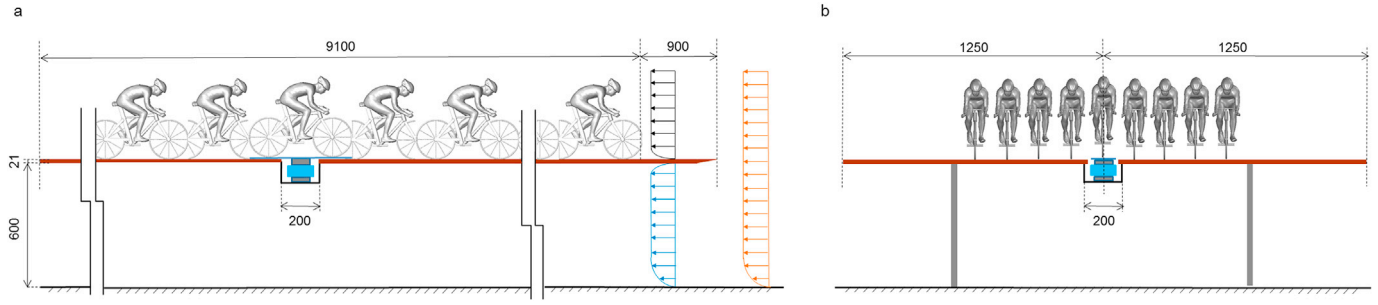

Fig. 11. Wind tunnel set-up at Eindhoven University of Technology for Peloton A with models on elevated sharp-edged plate to reduce boundary-layer thickness. Dimensions in mm.

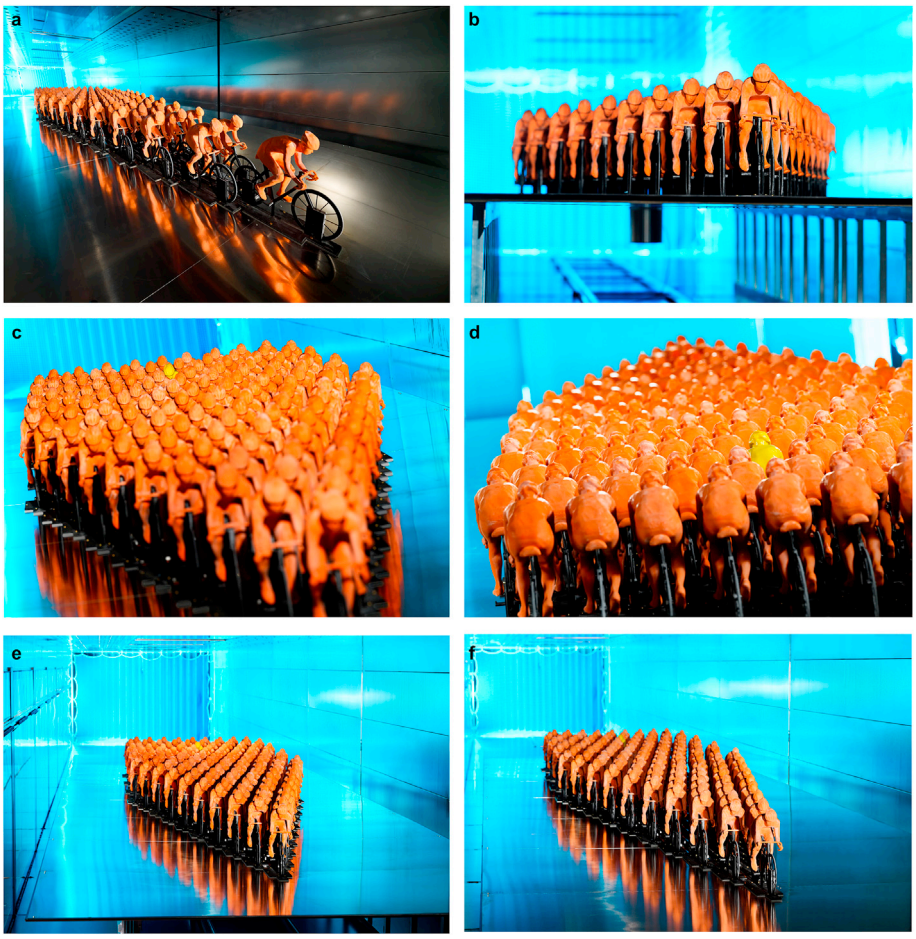

Fig. 12. Photographs of quarter-scale Peloton A model in wind tunnel.

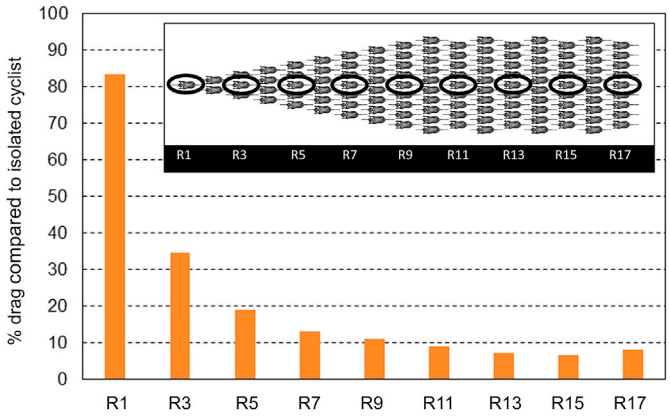

Fig. 13. Results from wind tunnel measurements: drag of the nine cyclists in the vertical centerplane as a percentage of the drag of an isolated cyclist riding at the same speed.

The riders in the last five rows have the lowest drag, that can go down to only 6% of that of the isolated rider. Similar to Peloton A, overall, the cyclists at the mid rear of the peloton have the strongest drag reductions. 48 of these riders have drag reductions down to 5–10% that of the isolated rider. This means that almost 40% of this peloton travels at very low cost in terms of energy. Although Peloton A and B have quite a different density due to different streamwise spacing between the riders, the drag values found in both are very similar, except for the leading rider. This suggests that these drag reductions are also representative of those in actual pelotons that have configurations/spacings generally between those of the denser Peloton A and the sparser Peloton B.

To further analyze the results, we define the parameter "equivalent cycling speed", which is the speed of an isolated rider that would yield the same drag as that of the rider at a given position in the peloton. For every rider in the peloton, the equivalent cycling speed can easily be determined given the square root relationship between wind speed and drag. For a peloton at 15 m/s speed, a reduction in drag down to 5% and 10% corresponds to an equivalent cycling speed of 3.35 m/s and 4.74 m/s, respectively. These values are 4.5 to 3.2 times lower than the peloton speed. The equivalent cycling speed can also be estimated from the CFD results, as it can be linked to the wind speed that approaches the cyclist, i.e. the wind speed ahead of the cyclist. Fig. 24a and b defines three vertical lines in front of each of the nine cyclists in the vertical centerplane. Fig. 24c shows the streamwise wind velocity component averaged over the three lines from 0 m (ground level) up to 1.6 m (just above helmet height). This parameter can also be averaged over this height yielding the values of $U_{X,AVG}$ that are also displayed in Fig. 24c. While the leading cyclist has an approach-flow wind speed a bit below the riding speed of 15 m/s (due to the subsonic upstream disturbance by this cyclist himself/herself and the riders behind him/her), the other riders see a much larger decrease of estimated approach-flow wind speed. For the last rider, the approach-flow wind speed (at P09) varies from slightly more than 6 m/s near ground level to just above 3 m/s at larger height, yielding an average value of 4.2 m/s. This corresponds fairly well to the equivalent cycling speed of 3.35 m/s, considering that the actual equivalent cycling speed is the result of a complex vector field in front of the cyclist where large lateral gradients can occur that not represented in the estimate in Fig. 24c.

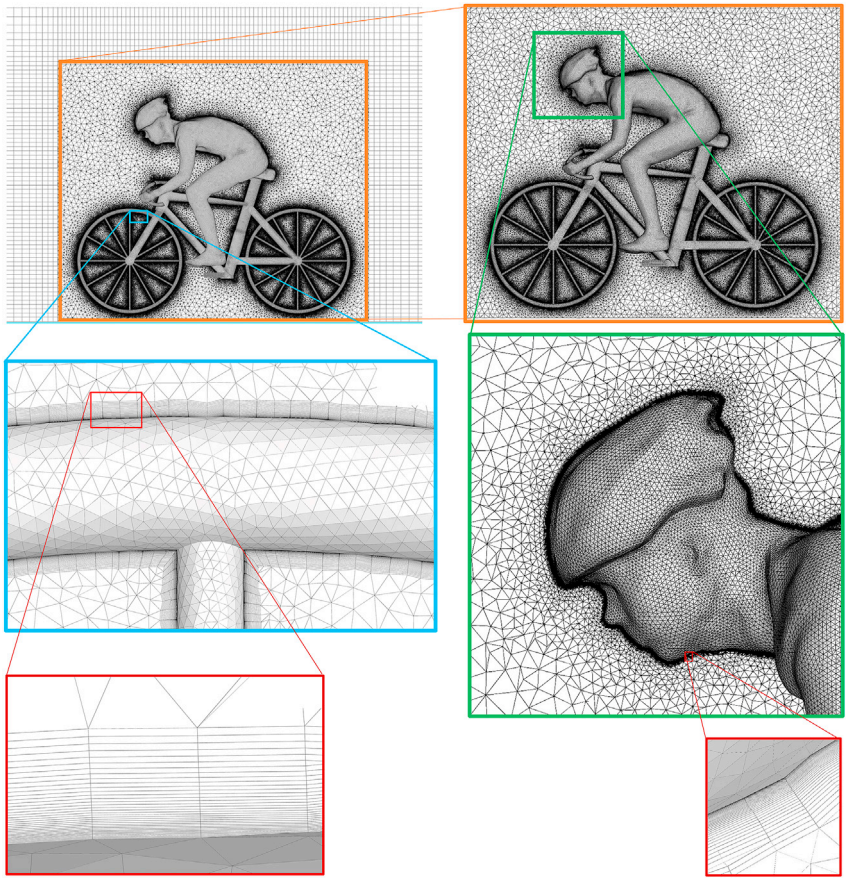

Fig. 14. Details of computational grid on and around the cyclist geometry, the wall-adjacent grid cell is 0.02 mm.

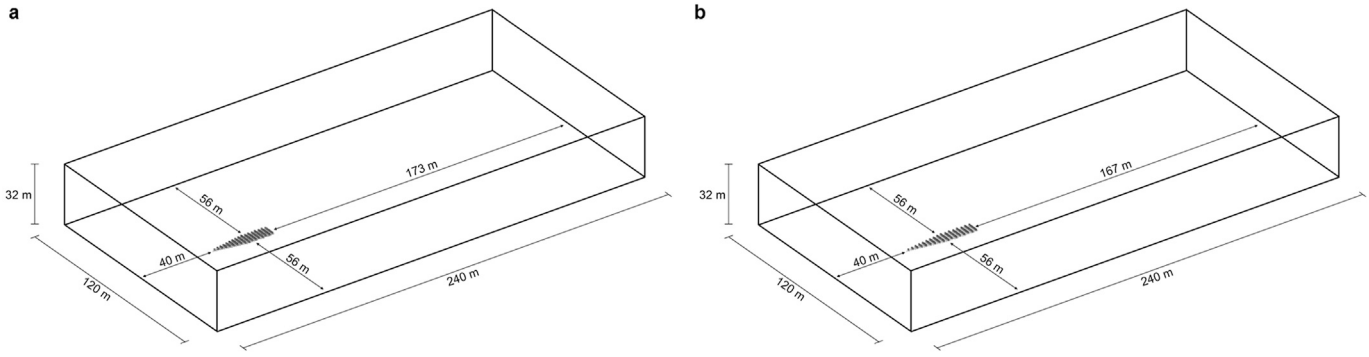

Fig. 15. Computational domains for (a) Peloton A and (b) Peloton B.

7. Discussion

7.1. Drag reductions down to 5–10% in this study versus 50–70% stated in the literature

The finding that the drag of a cyclist in the mid rear of a densely packed peloton goes down to 5%–10% of the drag of an isolated cyclist riding at the same speed is in strong contrast to the values of 50%–70% that have been mentioned in previous studies and that are implemented in state-of-the-art mathematical models of cycling (e.g. Gaul et al., 2018). The values of 50% and 70% originate from studies with small groups of in-line drafting riders. Indeed, as shown in Fig. 9, values of about 50%–70% are found for the trailing riders in such groups. However, the situation in a peloton is quite different. A cyclist in the mid rear of tightly packed peloton is sheltered from wind by multiple rows of riders in front of him/her (see Fig. 1) while also the many riders behind him/her provide an aerodynamic benefit because of the subsonic upstream disturbance. As a result, a larger drag reduction should be expected than obtained for simple in-line configurations of only a few riders. Indeed, a drag reduction down to 50% or 70% also does not correspond to the experience expressed by professional cyclists and practical cycling experts, who mentioned that "a cyclist situated in the belly of the peloton hardly has to pedal to move with the peloton and will have extremely low energy expenditure" (e.g. Bakelants, 2018; Wuyts and De Cauwer, 2018). Based on high-resolution CFD simulations validated with four different wind tunnel tests, the present study shows that the drag of the vast majority of cyclists in a peloton decreases much below the value of 50%. While the value of 5%–10% might appear very low, one should consider that this corresponds to an "equivalent cycling speed" of 3.35 m/s to 4.74 m/s when the peloton is riding at 15 m/s. This equivalent cycling

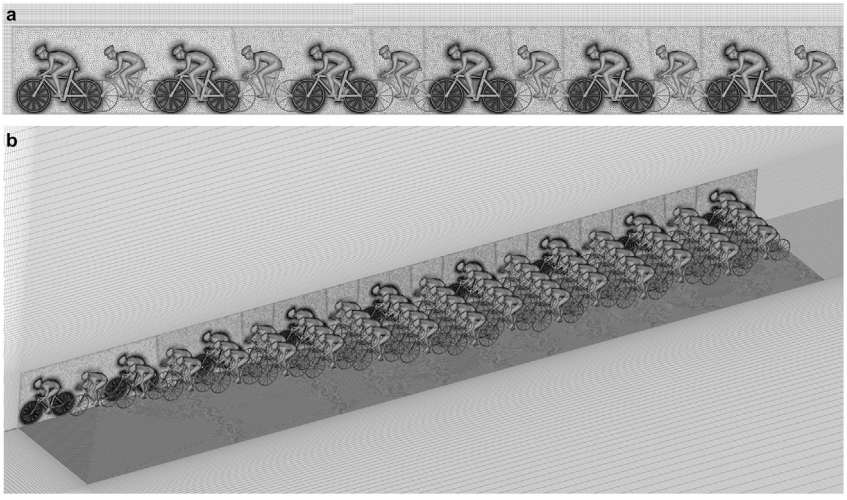

Fig. 16. Side and perspective view of computational grid on cyclists, ground surface and vertical centerplane for Peloton A: 2,979, 420, 781 cells.

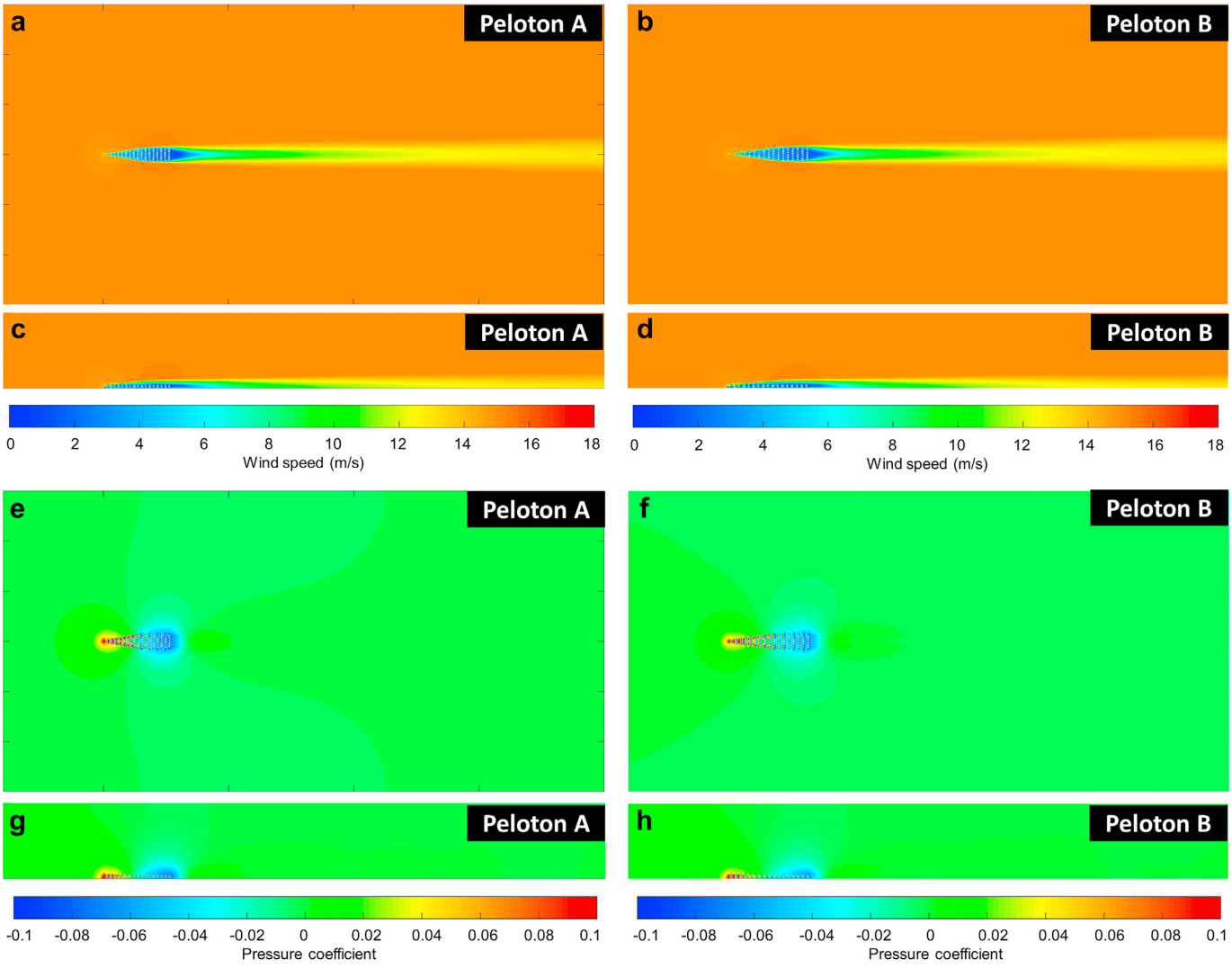

Fig. 17. Contours of (a–d) mean wind speed and (e–h) mean pressure coefficient for Pelotons A and B. (a,b,e,f) In a horizontal plane at 1 m above the road. (c,d,g,h) In the vertical centerplane.

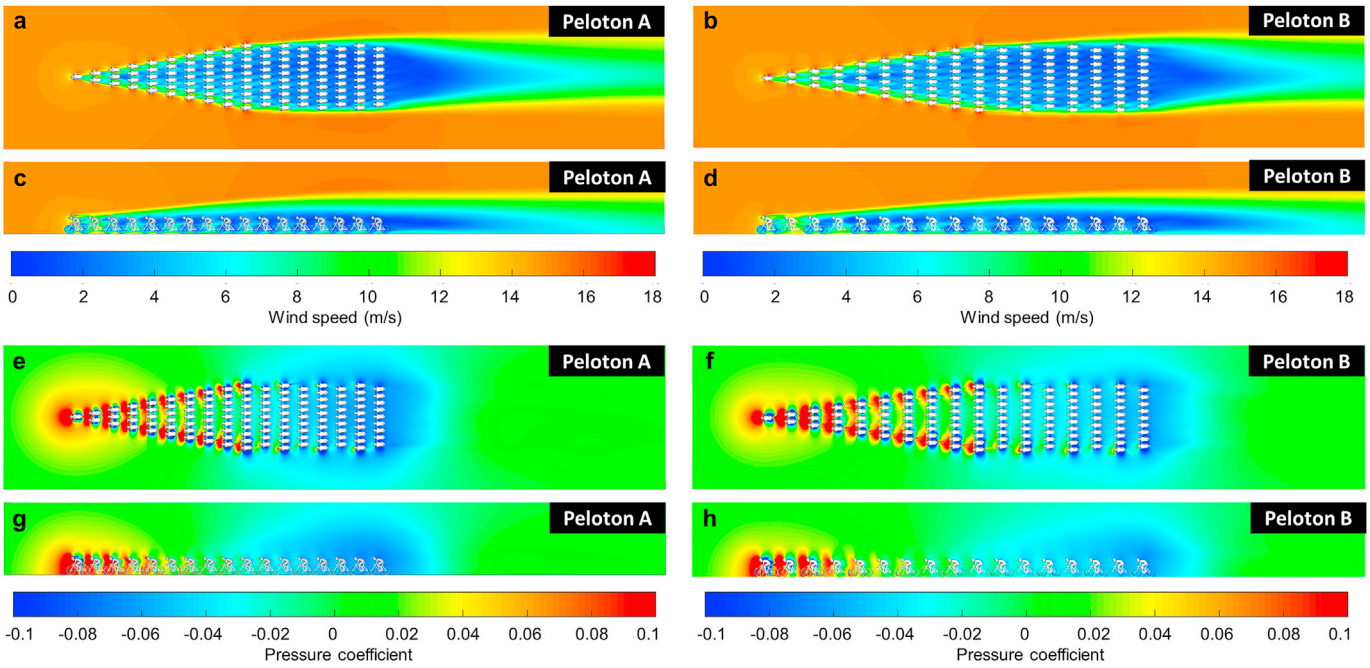

Fig. 18. Detailed view of (a–d) contours of mean wind speed and (e–h) mean pressure coefficient for Pelotons A and B. (a,b,e,f) In a horizontal plane at 1 m above the road. (c,d,g,h) In the vertical centerplane.

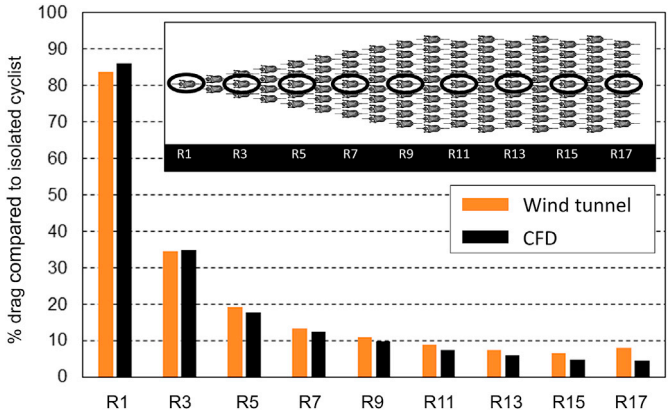

Fig. 19. Wind tunnel and CFD results of the drag of the nine cyclists along the centerline, expressed as a percentage of the drag of an isolated cyclist riding at the same speed.

speed is 4.5 and 3.2 times lower than the peloton speed. This value does correspond to the experience expressed by professional cyclists and practical cycling experts that riding in the belly of the peloton requires extremely low pedaling effort. Even though this experience has been around for a very long time, its contradiction with the values in the scientific literature indicate a substantial lack of knowledge about aerodynamic drag in cycling pelotons. Therefore, to the best of our knowledge, this study represents the first time that aerodynamic drag in the peloton has been systematically investigated. This study quantifies the drag reductions and shows which positions are most beneficial in terms of drag reduction. It also shows how much drag is experienced by the riders that are riding in front or at the outskirts of the peloton.

7.2. Limitations

Although this study is based on detailed CFD simulations and wind tunnel experiments for realistic cyclist geometries in two large pelotons, it is also subjected to a number of limitations. The cyclists, both in the CFD simulations and in the wind tunnel measurements, have static legs and the wheels are fixed. Earlier research has shown that the aerodynamic drag of a pedaling cyclist, averaged over one pedaling revolution, is quite similar to that of the same cyclist with the crank almost horizontal (Crouch et al., 2016). To obtain a first indication of the effect of rotating wheels, we perform one simulation of an isolated cyclist where the wheels are allowed to rotate corresponding to the cycling speed of 15 m/s. The moving reference frame method is employed (ANSYS, 2013). The geometry of the cyclist body is identical as in Fig. 2 but some parts of the bicycle and especially the wheels are modified to represent a more realistic actual wheel geometry with a larger number of thin spokes (Fig. 25). The resulting computational grid consists of 55.3 million cells (Figs. 25 and 26). The simulation set-up in terms of computational domain, boundary conditions, approximate forms of the governing equations, turbulence model etc. is identical as outlined above, however, averaging is performed over 11,000 time steps given the wheel rotation as complicating factor. The CFD simulation for the geometry in Fig. 25 with static wheels yields a drag force of 36.06 N, while the simulation for the same geometry with rotating wheels yields 37.30 N. This would indicate that wheel rotation is not a major factor in cycling aerodynamics, at least not for an isolated rider and in the absence of cross wind. However, a peloton configuration is much more complicated than that of an isolated cyclist and future research should investigate the effect of wheel rotation on aerodynamic drag in pelotons.

All CFD simulations and wind tunnel measurements in this study assumed that the cyclist(s) is/are riding in still air, so no head wind, tail wind or cross wind is present. Future research should investigate especially the effect of cross wind on peloton aerodynamics, which should consider different peloton shapes including the typical echelon that is formed at the front under cross-wind conditions (see Fig. 1g and h).

Other simplifications in this study include the steady-state calculations (in spite of the pseudo-transient approach) and the fact that we did not consider cyclists in the peloton moving throughout the peloton towards another position.

This study only focused on aerodynamic drag, which is the largest resistance for a cyclist riding at a typical racing speed (54 km/h, 15 m/s). However, as the aerodynamic drag is reduced for riders inside the peloton, the other components of the total resistance, such as rolling

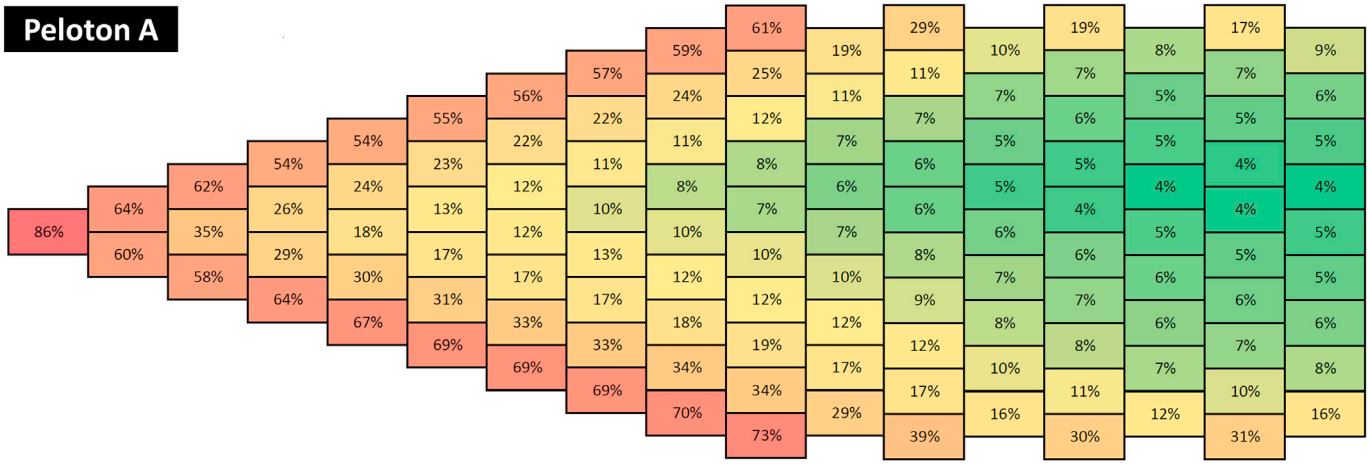

Fig. 20. Drag of every cyclist in Peloton A as a percentage of the drag of an isolated cyclist riding at the same speed.

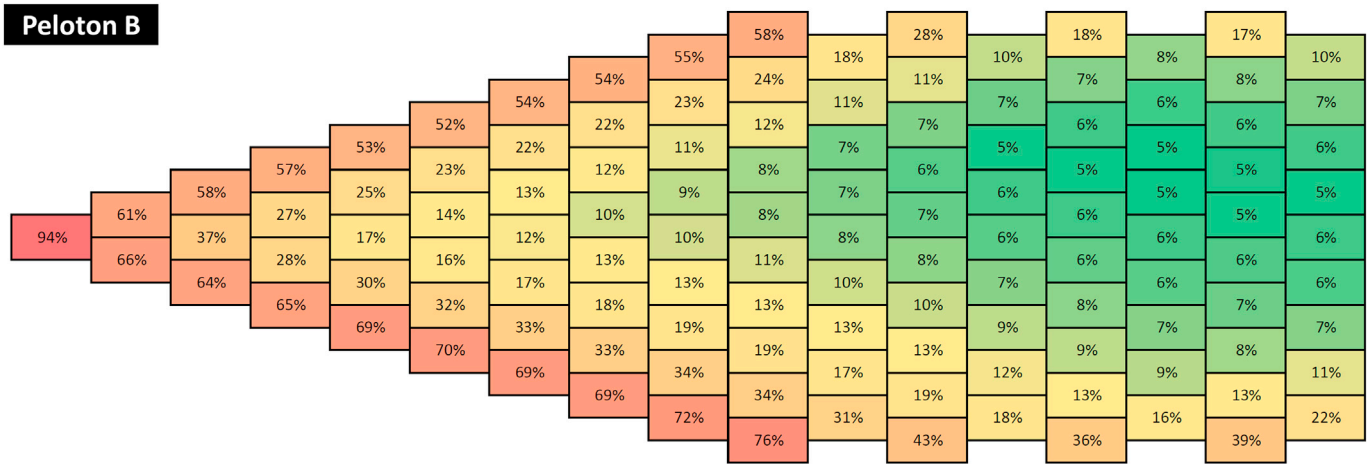

Fig. 21. Drag of every cyclist in Peloton B as a percentage of the drag of an isolated cyclist riding at the same speed.

resistance and wheel-bearing resistance will become relatively more important. Future research should combine all components of resistance to provide more complete information.

7.3. On the best position in the peloton

While the present study shows that the lowest aerodynamic drag in the pelotons that were studied is found in the last 4 or 5 rows, this position is not necessarily the best position considering all aspects in a cycling race. Riders at the end of the peloton will be less likely to see and react to attacks from competitors. They might miss a breakaway. If the peloton breaks into pieces, due to accelerations in the front part or due to a crash, they might get caught in the rear group and extra efforts will be needed to bridge the gap to the leading group, which might even be impossible. Finally, riders at the rear of the peloton are also more likely to be involved in crashes, both because there are more riders in front of them but also because of the so-called accordion effect, which refers to the amplification of changes in speed as they propagate to the back of the peloton. In this accordion, riders at the rear need to anticipate and brake early to avoid collisions when the front part of the peloton slows down. Conversely, when the front part of the peloton accelerates, riders at the end of the peloton will have to generate a larger acceleration than the others to close the gap between them and the others. A similar thing happens in case of bends, when the peloton will stretch out and this stretching will generally be larger further downstream the peloton. As a result, the best position in the peloton will generally not be in the last four to five last, but more in front, but nevertheless still sufficiently shielded by others, such as position R4 or R5 in Fig. 19, and where the leaders will generally be surrounded by members of their team, at least in the most critical parts of the race.

7.4. Similarities in nature

There are numerous examples in nature where animals travel in groups in ways that have been proven or at least expected to yield reductions in energy expenditure. Fish (1995) analyzed the kinematics of the paddling stroke of ducklings swimming in formation to detect differences in relation to swimming effort and position in the formation. His results suggest that mechanical energy is conserved when formation swimming is employed. Weihs (2004) analyzed the hydrodynamic interaction between a mother dolphin and a nearby calf demonstrating the benefits in terms of energy expenditure for the calf. Williams et al. (1992) outlined how trained dolphins take hydrodynamic benefit to save energy by exploiting the water movements generated by boats. Weihs (1975) suggested that fish in a school may be able to benefit from each other's wakes, while Svendsen et al. (2003) demonstrated that fish swimming at the rear of a school beat their tails at frequencies around 10% lower than the leading fish in the school, suggesting that they were using less energy than the leading fish. Also birds flying in V-formation or in an oblique line benefit from this formation, as they take advantage of the wing tip vortices of the bird flying in front of them. In experiments with pelicans trained to follow a boat or an ultra-light plane,

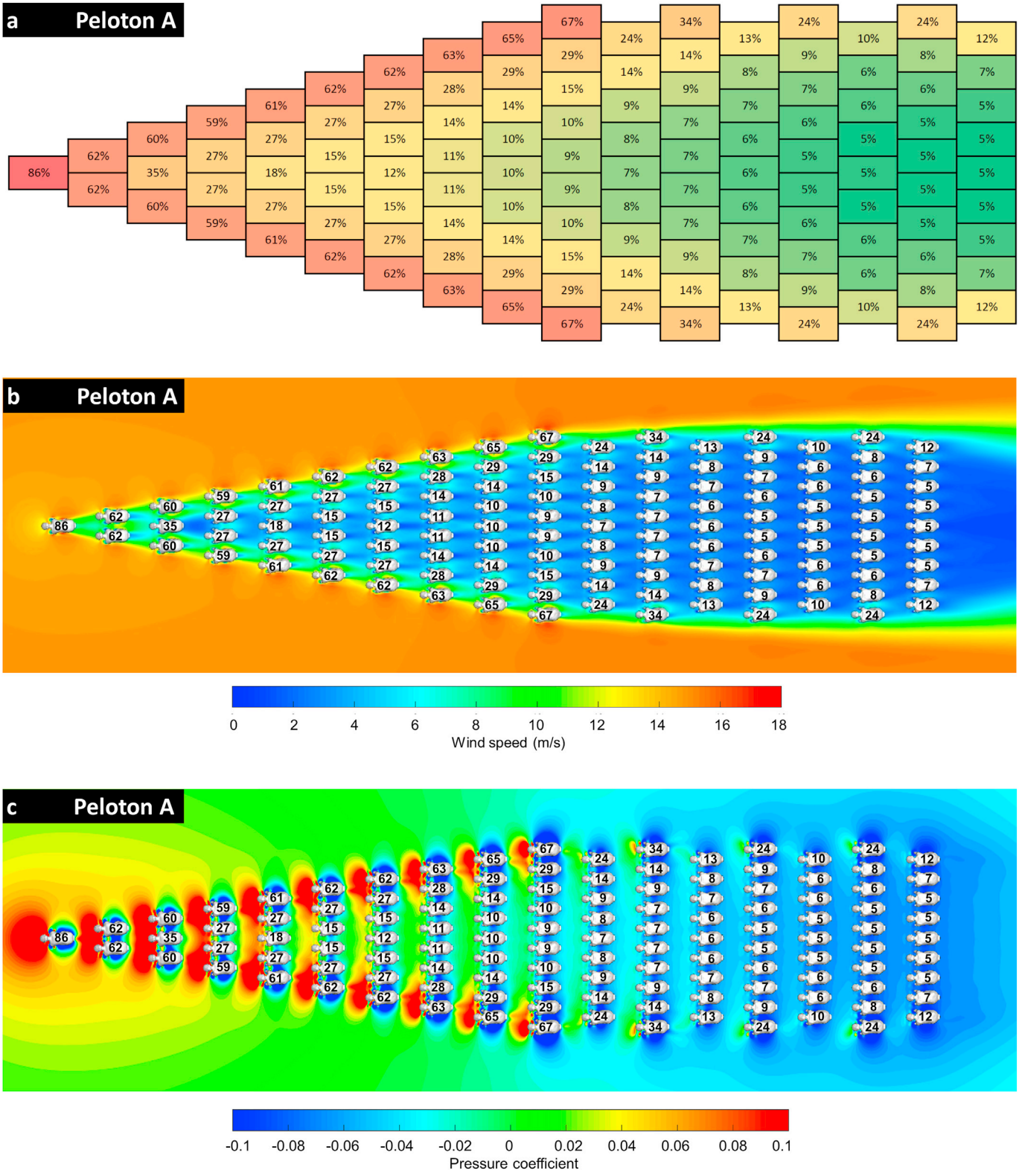

Fig. 22. Estimate of revolution-averaged drag of every cyclist in Peloton A as a percentage of the drag of an isolated cyclist riding at the same speed. Background of the figures (b) and (c) are contours in a horizontal plane at 1 m height of mean wind speed (m/s) and mean pressure coefficient, respectively.

Weimerskirch et al. (2001) showed that birds flying in third position or further back in a formation had heart rates around 13% lower than birds flying alone; the leader of the formation had about the same wing beat frequency as a solitary bird, but birds further back in the formation beat their wings at lower frequencies. In reviewing these mechanisms of energy saving in nature, McNeill Alexander (2004) also briefly made the link to cycling where, he argued, similar benefits are obtained by drafting.

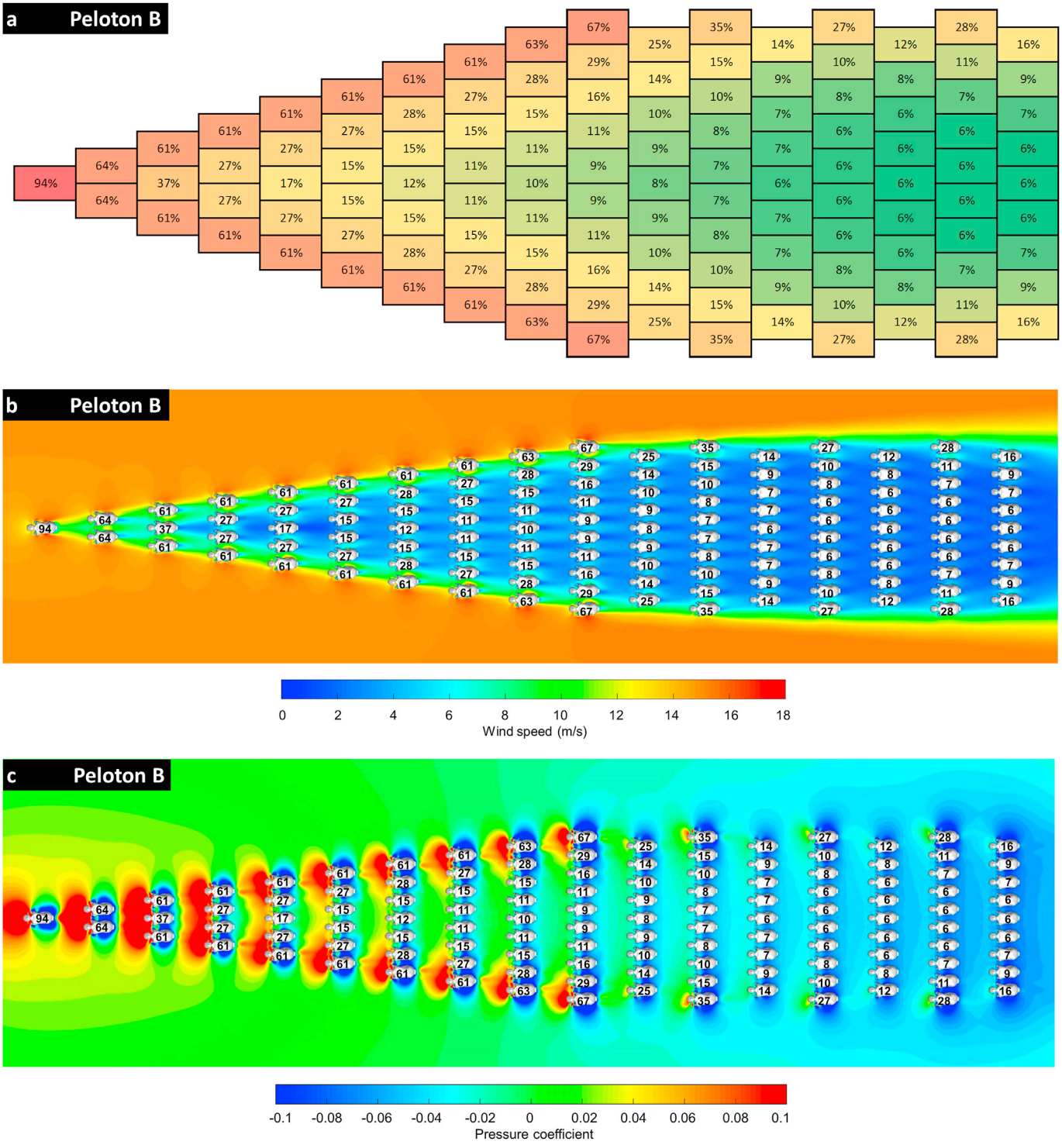

Fig. 23. Estimate of revolution-averaged drag of every cyclist in Peloton B as a percentage of the drag of an isolated cyclist riding at the same speed. Background of the figures (b) and (c) are contours in a horizontal plane at 1 m height of mean wind speed (m/s) and mean pressure coefficient, respectively.

8. Summary and conclusions

A cycling peloton is the main group of cyclists riding closely together to reduce aerodynamic drag and energy expenditure. While it is well known that the rider in front experiences the largest drag and riders well embedded in the peloton experience a large drag reduction, to the best of our knowledge, it was not yet known how large this drag reduction actually is and which drag reduction is obtained at which position in the peloton. It was also not known how much drag is experienced by the riders in front and at the outskirts of the peloton.

In the literature, it is stated that the aerodynamic drag in a cycling peloton can go down to 70 or even 50% that of an isolated cyclist riding at the same speed. These values are also used in mathematical models for cycling and breakaway strategies. They are based on drag investigations for small in-line groups of drafting cyclists. However, for a cyclist in the mid rear of a tightly packed peloton with multiple rows of riders

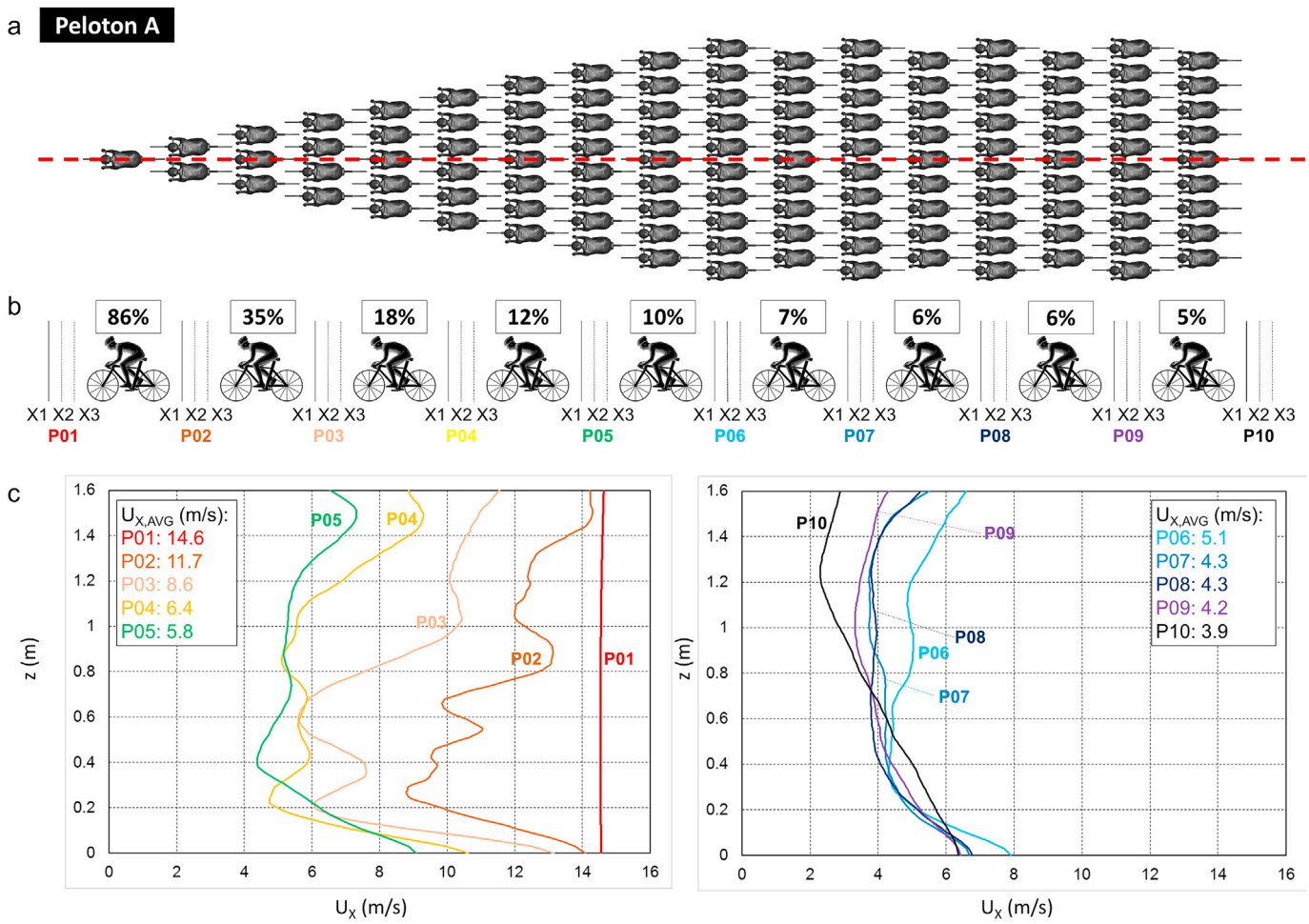

Fig. 24. Approach-flow wind speed U_X for the nine cyclists in the vertical centerplane in peloton A. Cycling speed is 15 m/s.

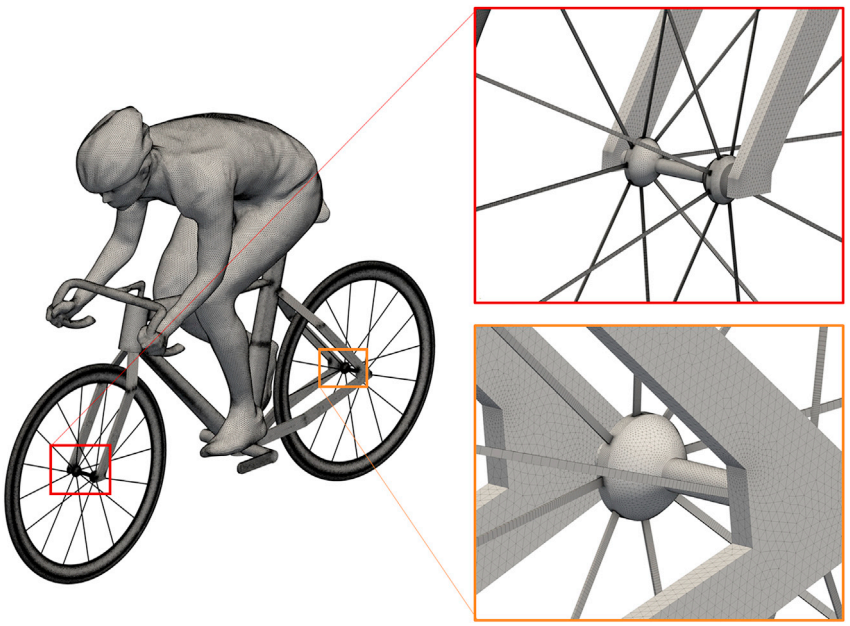

Fig. 25. Part of computational grid on cyclist surface with details of grid topology near wheel hub. Cell count: 55.3 million.

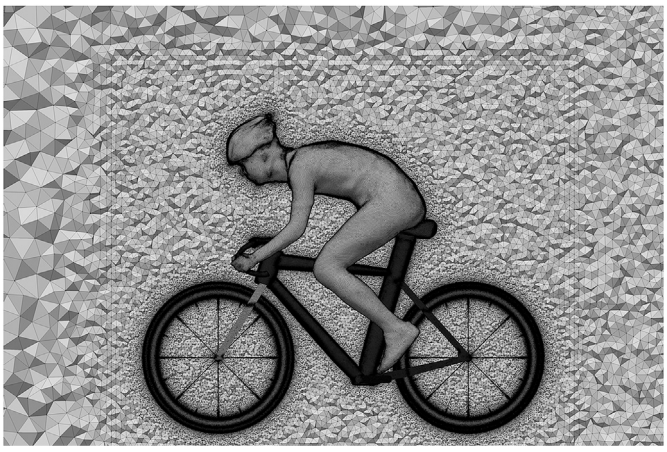

Fig. 26. Computational grid in vertical center plane. Cell count: 55.3 million.

providing shelter from wind, a larger drag reduction can be expected. Indeed, this is also indicated by professional cyclists and practical cycling experts, who mention that "a cyclist situated in the belly of the peloton hardly has to pedal to move with the peloton and will have extremely low energy expenditure". The present study was aimed at removing this apparent contradiction and to provide new insights into the distribution of aerodynamic drag in cycling pelotons by a combination of CFD simulation and wind tunnel testing.

To the best of our knowledge, studies of aerodynamic drag in large groups of drafting cyclists such as pelotons had not yet been performed. This paper therefore systematically investigated the aerodynamic drag for every rider in two pelotons of 121 cyclists. The pelotons had two different densities. It was assumed that there is no cross wind or strong head or tail wind and all cyclists were in dropped position. High-resolution CFD simulations were performed with the 3D Reynolds-averaged Navier-Stokes (RANS) equations and the Transition SST k-ω model. The stringent grid topology requirements for accurate cycling aerodynamics studies imposed the need for wall-adjacent cell sizes of 20 μm, which resulted in computational grids of nearly 3 billion cells. The CFD simulations were performed on supercomputers and the results were validated by four different wind tunnel tests, including one for a peloton of 121 quarter-scale models.

The wind tunnel and CFD results showed a similar trend of rapidly reducing drag of the riders in the vertical centerplane of the pelotons. While the agreement between wind tunnel and CFD results was very close for the first five riders in this centerplane, larger deviations were found for the last four riders in the centerplane, which was attributed to the complexity of the airflow pattern of multiple shear layers and wakes, which increases towards the rear of the peloton. Nevertheless, both wind tunnel and CFD results indicate that for the last 4 riders, the drag reduces down to 10 to 5% that of the isolated cyclist. Also the leading rider experiences a drag reduction, due to the upstream flow disturbance caused by the 120 riders behind him/her.

Analyzing the drag at all 121 positions showed that all cyclists in the peloton experience a drag reduction compared to an isolated cyclist riding at the same speed. The leading rider has the largest drag (84% and 96% of that of the isolated rider for Pelotons A and B, respectively), followed by the cyclists at the outer front edges of the peloton who have a drag reduction to a value in the range of 59–67%. For riders sufficiently embedded inside the peloton, the aerodynamic drag reduces strongly. Overall, the cyclists at the mid rear of the peloton have the largest drag reductions. For Peloton A, 57 of these riders have drag reductions down to 5–10% that of the isolated rider. This means that almost half of this peloton travels at very low cost in terms of energy. For Peloton B, 48 of these riders have drag reductions down to 5–10% that of the isolated rider. This means that almost 40% of this peloton travels at very low cost in terms of energy. Hence, the peloton is a very energy-efficient transport mechanism. Although Pelotons A and B have quite a different density due to different streamwise spacing between the riders, the drag values found in both are very similar, except for the leading rider. This suggests that these drag reductions – except for the leading rider – also represent those occurring in actual pelotons that have configurations/spacings generally between those of the denser Peloton A and the sparser Peloton B.

The "equivalent cycling speed" was defined as the virtual speed of an isolated rider that would yield the same drag as that of a rider at a given position in the peloton. For a peloton at 15 m/s speed, a reduction in drag down to 10 or 5% corresponds to an equivalent cycling speed of 4.74 m/s and 3.35 m/s, respectively. These values are 3.2–4.5 times lower than the peloton speed. These numbers correspond better to the statement by cycling professionals and practical cycling experts that "a cyclist situated in the belly of the peloton hardly has to pedal to move with the peloton and will have extremely low energy expenditure". In spite of the knowledge embedded in this statement, this study has increased the knowledge of aerodynamic drag in cycling pelotons by determining the actual drag reductions and their distribution inside the peloton. This study has shown that in a peloton, every rider benefits, and that the most substantial drag reductions are obtained by riders in the mid rear of the peloton. These results can be used to improve cycling strategies including breakaways and energy saving for the final sprint. They can also be used to improve the reliability of mathematical models of cycling that are also sometimes employed to develop breakaway strategies.

Acknowledgements

The work in this paper has been made possible by supercomputing with ANSYS Fluent CFD software on Cray supercomputers. The authors gratefully acknowledge the collaboration with ANSYS (Wim Slagter, Rongguang Jia, Shriram Jagannathan) and CRAY (Jef Dawson, David Whitaker) for running the peloton simulation jobs. This work was also sponsored by NWO Exacte en Natuurwetenschappen (Physical Sciences) for the use of supercomputer facilities, with financial support from the Nederlandse Organisatie voor Wetenschappelijk Onderzoek (Netherlands Organisation for Scientific Research, NWO) for the sub-configuration validation studies. The authors are very grateful to Custom Company (Jaspal Bathal), FlexForm (Frank Broos) and Tenax (Ronnie van Grunsven) for the efficient casting of the 121 high-quality cyclist models for the wind tunnel tests conducted at Eindhoven University of Technology. The authors thank ANSYS for contributing to the model casting costs. The authors are also very grateful to the anonymous reviewers for their very valuable and constructive comments on this paper.

References

Artec Europe, 2017. Artec Eva, 3D scanners. Retrieved May 22, 2017, from. https://www.artec3d.com/3d-scanner/artec-eva.
ANSYS Fluent, 2015. ANSYS Fluent Theory Guide. Release 16.1 Documentation. ANSYS Inc.
Bakelants, J., 2018. Personal Communication.
Baker, C.J., 2007. Wind engineering – past, present and future. J. Wind Eng. Ind.
Barlow, J.B., Rae, W.H., Pope, A., 1999. Low-speed Wind Tunnel Testing, third ed. Wiley.
Barry, N., Burton, D., Sheridan, J., Thompson, M., Brown, N.A.T., 2015. Aerodynamic drag interactions between cyclists in a team pursuit. Sports Eng. 18 (2), 93–103.
Blocken, B., 2014. 50 years of computational wind engineering: past, present and future. J. Wind Eng. Ind. Aerod. 129, 69–102.
Blocken, B., 2015. Computational Fluid Dynamics for Urban Physics: importance, scales, possibilities, limitations and ten tips and tricks towards accurate and reliable simulations. Build. Environ. 91, 219–245.
Blocken, B., Carmeliet, J., 2008. Pedestrian wind conditions at outdoor platforms in a high-rise apartment building: generic sub-configuration validation, wind comfort assessment and uncertainty issues. Wind Struct. 11 (1), 51–70.
Blocken, B., Toparlar, Y., 2015. A following car influences cyclist drag: CFD simulations and wind tunnel measurements. J. Wind Eng. Ind. Aerod. 145, 178–186.
Blocken, B., Janssen, W.D., van Hooff, T., 2012. CFD simulation for pedestrian wind comfort and wind safety in urban areas: general decision framework and case study for the Eindhoven University campus. Environ. Model. Software 30, 15–34.
Blocken, B., Defraeye, T., Koninckx, E., Carmeliet, J., Hespel, P., 2013. CFD simulations of the aerodynamic drag of two drafting cyclists. Comput. Fluids 71, 435–445.
Blocken, B., Toparlar, Y., Andrianne, T., 2016. Aerodynamic benefit for a cyclist by a following motorcycle. J. Wind Eng. Ind. Aerod. 155, 1–10.

Broker, J.P., Kyle, C.R., 1995. Pursuit Aerodynamics, Project96: Wind Tunnel Test Results. USOC Sport Science and Technology Report. Colorado Springs, pp. 1–46 (from Basset et al., 1999).
Broker, J.P., Kyle, C.R., Burke, E.R., 1999. Racing cyclist power requirements in the 4000-m individual and team pursuits. Med. Sci. Sports Exerc. 31 (11), 1677–1685.
Burke, E.R., 2003. High-tech Cycling, second ed. Human Kinetic Publishers, p. 328.
Casey, M., Wintergerste, T., 2000. Best Practice Guidelines. ERCOFTAC Special Interest Group on "Quality and Trust in Industrial CFD", ERCOFTAC.
Crouch, T.N., Burton, D., Brown, N.A.T., Thomson, M.C., Sheridan, J., 2014. Flow topology in the wake of a cylist and its effect on aerodynamic drag. J. Fluid Mech. 748, 5–35.
Crouch, T.N., Burton, D., Thompson, M.C., Brown, N.A.T., Sheridan, J., 2016. Dynamic leg-motion and its effect on the aerodynamic performance of cyclists. J. Fluid Struct. 65, 121–137.
Crouch, T.N., Burton, D., LaBry, Z.A., Blair, K.B., 2017. Riding against the wind: a review of competition cycling aerodynamics. Sports Eng. 20 (2), 81–110.
Dal Monte, A., Leonardi, L.M., Menchinelli, C., Marini, C., 1987. A new bicycle design based on biomechanics and advanced technology. Int. J. Sport Biomechan. 3, 287–292.
Defraeye, T., Blocken, B., Koninckx, E., Hespel, P., Carmeliet, J., 2010a. Aerodynamic study of different cyclist positions: CFD analysis and full-scale wind-tunnel tests. J. Biomech. 43 (7), 1262–1268.
Defraeye, T., Blocken, B., Koninckx, E., Hespel, P., Carmeliet, J., 2010b. Computational Fluid Dynamics analysis of cyclist aerodynamics: performance of different turbulence-modelling and boundary-layer modelling approaches. J. Biomech. 43 (12), 2281–2287.
Defraeye, T., Blocken, B., Koninckx, E., Hespel, P., Verboven, P., Nicolai, B., Carmeliet, J., 2014. Cyclist drag in team pursuit: influence of cyclist sequence, stature, and arm spacing. J. Biomech. Eng. ASME 136 (1) art. no. 011005.
Edwards, A.G., Byrnes, W.C., 2007. Aerodynamic characteristics as determinants of the drafting effect in cycling. Med. Sci. Sports Exerc. 39 (1), 170–176.
Fintelman, D.M., Sterling, M., Hemida, H., Li, F.X., 2014. The effect of crosswinds on cyclists: an experimental study. The Engineering of Sport 10. Procedia Eng. 72, 720–725.
Fintelman, D.M., Hemida, H., Sterling, M., Li, F.X., 2015. CFD simulations of the flow around a cyclist subjected to crosswinds. J Wind Eng Aerod. 144, 31–41.
Fish, F.E., 1995. Kinematics of ducklings swimming in formation: consequences of position. J. Exp. Zool. 273 (1), 1–11. https://doi.org/10.1002/jez.1402730102.
Franke, J., Hellsten, A., Schlünzen, H., Carissimo, B., 2007. Best Practice Guideline for the CFD Simulation of Flows in the Urban Environment, COST Action 732: Quality Assurance and Improvement of Microscale Meteorological Models, Hamburg, Germany.
Garcia-Lopez, J., Rodriguez-Marroyo, J.A., Juneau, C.E., Peleteiro, J., Martinez, A.C., Villa, J.G., 2008. Reference values and improvement of aerodynamic drag in professional cyclists. J. Sports Sci. 26 (3), 277–286.
Gaul, L.H., Thomson, S.J., Griffiths, I.M., 2018. Optimizing the breakaway position in cycle races using mathematical modelling. Sports Eng. https://doi.org/10.1007/s12283-018-0270-5.
Gore, M., 2016. Personal Communication with Sensor Manufacturer.
Grappe, G., Candau, R., Belli, A., Rouillon, J.D., 1997. Aerodynamic drag in field cycling with special reference to the Obree's position. Ergonomics 40 (12), 1299–1311.
Hagberg, J.M., McCole, S.D., 1990. The effect of drafting and aerodynamic equipment on the energy expenditure during cycling. Cycl. Sci. 2 (3), 19–22.
Jeukendrup, A.E., Martin, J., 2001. Improving cycling performance: how should we spend our time and money. Sports Med. 31 (7), 559–569.
Kyle, C.R., 1979. Reduction of wind resistance and power output of racing cyclists and runners travelling in groups. Ergonomics 22 (4), 387–397.
Kyle, C.R., 1991. The effects of cross winds upon time trails. Cycl. Sci. 3 (3–4), 51–56 (from Basset et al., 1999).
Kyle, C.R., Burke, E.R., 1984. Improving the racing bicycle. Mech. Eng. 106 (9), 34–45.
Langtry, R.B., Menter, F.R., 2009. Correlation-based transition modeling for unstructured parallelized computational fluid dynamics codes. AIAA J. 47 (12), 2894–2906.
Lukes, R.A., Chin, S.B., Haake, S.J., 2005. The understanding and development of cycling aerodynamics. Sports Eng. 8, 59–74.
Mannion, P., Toparlar, Y., Blocken, B., Hajdukiewicz, M., Andrianne, T., Clifford, E., 2018a. Improving CFD prediction of drag on Paralympic tandem athletes: influence of grid resolution and turbulence model. Sports Eng. 21 (2), 123–135.
Mannion, P., Toparlar, Y., Blocken, B., Clifford, E., Andrianne, T., Hajdukiewicz, M., 2018b. Aerodynamic drag in competitive tandem para-cycling: road race versus time-trial positions. J. Wind Eng. Ind. Aerod. 179, 92–101.
Martin, J.C., Milliken, D.L., Cobb, J.E., McFadden, K.L., Coggan, A.R., 1998. Validation of a mathematical model for road cycling power. J. Appl. Biomech. 14, 276–291.
McCole, S.D., Claney, K., Conte, J.-C., Anderson, R., Hagberg, J.M., 1990. Energy expenditure during bicycling. J. Appl. Physiol. 68 (2), 748–753.
McNeill Alexander, R., 2004. Hitching a lift hydrodynamically - in swimming, flying and cycling. J. Biol. 3 (2), 7. https://doi.org/10.1186/jbiol5.
Menter, F.R., Langtry, R., Volker, S., 2006. Transition modelling for general purpose CFD codes. Flow, Turbul. Combust. 77 (1), 277–303.
Meroney, R.N., Derickson, R., 2014. Virtual reality in wind engineering: the windy world within the computer. J. Wind Eng. 11 (2), 11–26.
Murakami, S., 1997. Current status and future trends in computational wind engineering. J. Wind Eng. Ind. Aerod. 67 and 68, 3–34.
Olds, T., 1998. The mathematics of breaking away and chasing in cycling. Eur. J. Appl. Physiol. 77, 492–497.
Padilla, S., Mujika, I., Angulo, F., Goiriena, J.J., 2000. Scientific approach to the 1-h cycling world record: a case study. J. Appl. Physiol. 89, 1522–1527.
Ratamero, E.M., 2015. Modelling peloton dynamics in competitive cycling: a quantitative approach. In: Sports Science Research and Technology Support, ICSPORTS, Book Series Communications in Computer and Information Science, 464, pp. 42–56.
Solari, G., 2007. The international association for wind engineering (IAWE): Progress and prospects. J. Wind Eng. Ind. Aerod. 95, 813–842.
Stathopoulos, T., 1997. Computational wind engineering: past achievements and future challenges. J. Wind Eng. Ind. Aerod. 67–68, 509–532.
Svendsen, J.C., Skov, J., Bildsoe, M., Steffensen, J.F., 2003. Intra-school positional preference and reduced tail beat frequency in trailing positions in schooling roach under experimental conditions. J. Fish. Biol. 62, 834–846. https://doi.org/10.1046/j.1095-8649.2003.00068.x.
Tominaga, Y., Mochida, A., Yoshie, R., Kataoka, H., Nozu, T., Yoshikawa, M., Shirasawa, T., 2008. AIJ guidelines for practical applications of CFD to pedestrian wind environment around buildings. J. Wind Eng. Ind. Aerod. 96 (10–11), 1749–1761.
Tucker, P.G., Mosquera, A., 2001. NAFEMS Introduction to Grid and Mesh Generation for CFD. NAFEMS CFD Working Group. R0079, 56 pp.
Weihs, D., 1975. Some Hydrodynamical Aspects of Fish Schooling. In: Wu, T.Y., Brokaw, C.J., Brennen, C. (Eds.), In Swimming and Flying in Nature, 1975. Plenum Press, New York, pp. 703–718.
Weihs, D., 2004. The hydrodynamics of dolphin drafting. J. Biol. 3 (2), 8.
Weimerskirch, H., Martin, J., Clerquin, Y., Alexandre, P., Jiraskova, S., 2001. Energy saving in flight formation. Nature 413, 697–698. https://doi.org/10.1038/35099670.
Williams, T.M., Friedl, W.A., Fong, M.L., Yamada, R.M., Sedivy, P., Haun, J.E., 1992. Travel at low energetic cost by swimming and wave-riding bottlenose dolphins. Nature 355 (6363), 821–823.
Wilson, D.G., 2004. Bicycling Science, third ed. MIT Press, Cambridge, MA.
Wuyts, M., De Cauwer, J., 2018. Professional Cycling Reporters, Statements during Paris-Roubaix on Flemish Television, Sporza.Be, 8 April 2018.
Zdravkovich, M.M., Ashcroft, M.W., Chisholm, S.J., Hicks, N., 1996. Effect of cyclist's posture and vicinity of another cyclist on aerodynamic drag. In: Haake (Ed.), The Engineering of Sport. Balkema, Rotterdam, pp. 21–28.